The averaged dynamics of the hydrogen atom in crossed electric and magnetic fields as a perturbed Kepler problem[*]

Nils Berglund[†]and Turgay Uzer
School of Physics, Georgia Tech
Atlanta, GA 30332-0430, USA

July 13, 2000

Abstract

We treat the classical dynamics of the hydrogen atom in perpendicular electric and magnetic fields as a celestial mechanics problem. By expressing the Hamiltonian in appropriate action–angle variables, we separate the different time scales of the motion. The method of averaging then allows us to reduce the system to two degrees of freedom, and to classify the most important periodic orbits.

1   Introduction

Our contribution to this Special Issue lies at the intersection of Martin Gutzwiller's scientific interests, namely celestial mechanics, electron motion, and chaos, especially its manifestations in quantal systems. We will be performing "celestial mechanics on a microscopic scale" [U&91] by treating the dynamics of highly excited ("Rydberg") electrons [C98] in crossed electric and magnetic fields using classical mechanics.

Rydberg atoms in strong external fields constitute fundamental physical systems where the quantum mechanical regime of strong nonlinearity can be tested [G90, KvL95]. While the problem of a Rydberg atom interacting with a strong magnetic field (the Diamagnetic Kepler Problem, DKP, also known as the Quadratic Zeeman Effect, QZE) has been fairly well understood as a result of sustained research in the past two decades [HRW89, FrWi89], the superficially similar scenario resulting from the addition of a perpendicular electric field – the so-called crossed field arrangement [S83, BS84, W&89, RFW91, vMDU94, vMU97a] – remains the least understood of all Rydberg problems. This is all the more remarkable in view of the prominence of the crossed fields in diverse areas of physics ranging from excitonic systems to plasmas and neutron stars. This problem is so complex because no continuous symmetry survives the extensive symmetry breaking [DG89] induced by the two fields. The result is a wealth of new physics which is only possible beyond two degrees of freedom, such as Arnol'd diffusion [TLL79, G90, LL92, vMDU96]. This absence of symmetry also allows localizing electronic wavepackets in all spatial dimensions, and the observation of these localized wavepackets [Y&93] has led to new insights into the

---

[*]Dedicated to Martin C. Gutzwiller on the occasion of his 75th birthday.
[†]Present address: Weierstraß Institut, Mohrenstraße 39, D-10117 Berlin, Germany

dynamics of the electron in the correspondence principle regime. It has also been found that a velocity-dependent, Coriolis-like force in Newton's equations causes the ionization of the electron to exhibit chaotic scattering [MW92, UF95, JFU99]. All these phenomena, as well as renewed interest in the motional Stark effect [JHY83, F94], make the crossed-fields problem an experimental accessible paradigm for a wide variety of outstanding issues in atomic and molecular physics, solid-state physics [DS92, Schm93], nuclear physics [BM75], astrophysics [Ma89], and celestial mechanics [Mi82].

The experimental challenge has been taken up by Raithel, Fauth, and Walther [RFW91, RFW93] who in a landmark series of experiments have identified a class of quasi-Landau (QL) resonances in the spectra of rubidium Rydberg atoms in crossed electric and magnetic fields. Similar to the original QL resonances observed by Garton and Tomkins [GT69], this set of resonances is associated with a rather small set of *planar* orbits of the crossed-fields Hamiltonian which is known to support an enormous number of mostly non-planar periodic motions [RFW91]. The dominance of planar orbits in these experiments has recently been explained [vMFU97a].

In contrast with the DKP, and despite some preliminary work [FlWe96], the systematics of periodic orbits in the crossed-fields problem has not been discovered up to now. The aim of the present work is to initiate a systematic classification of the orbits of the crossed-fields Hamiltonian, based on methods developed in celestial mechanics, specifically Delaunay variables and averaging. The analogy between atomic and planetary systems was already used by Born [B27], who studied in particular the crossed-fields problem, but neglected the quadratic Zeeman term because he was not studying Rydberg atoms, where it is prominent.

Delaunay variables are action–angle variables which have a clear geometric interpretation in terms of Kepler ellipses. A fascinating historical account of the developments in celestial mechanics leading to the introduction of Delaunay variables can be found in a recent review by Gutzwiller [G98]. These variables allow to separate the time scales of the motion, which is represented as a fast rotation of the planet (or the electron), along a Kepler ellipse with slowly changing orientation and eccentricity.

The technique of averaging [V96] allows to decrease the number of degrees of freedom by eliminating the fast motion along the Kepler ellipse. It has been used for a long time in celestial mechanics to compute the so-called secular motion of the solar system, and can be considered as a first order perturbation theory [D69, H70]. A systematic use of averaging allowed Laskar to integrate the motion of the solar system over several hundred million years [L90, L96, LR93]. The method has been applied to the DKP in [DKN83, CDMW87].

We note in passing that the direct connection to celestial mechanics that the Delaunay variables provide is lost with an alternative set of variables called the Lissajous elements. These are obtained by regularizing the Coulomb Hamiltonian [F&92], and are appropriate for investigating the level structure of Rydberg atoms. The connection between the two sets in two dimensions is given by [DW91].

In this paper, we use the following notations. The Hamiltonian of an electron subjected to a Coulomb potential, a magnetic field $\mathbf{B}$ and an electric field $\mathbf{F}$ can be written in dimensionless units as

$$H(p_x, p_y, p_z; x, y, z) = \frac{1}{2}p^2 - \frac{1}{r} + \frac{1}{2}\mathbf{L} \cdot \mathbf{B} + \frac{1}{8}(\mathbf{r} \wedge \mathbf{B})^2 - \mathbf{r} \cdot \mathbf{F}, \qquad (1)$$

where $\mathbf{r} = (x, y, z)$ is the electron's position, $\mathbf{p} = (p_x, p_y, p_z)$ its momentum, and $\mathbf{L} = \mathbf{r} \wedge \mathbf{p}$ its angular momentum. We write $r = \|\mathbf{r}\|$ and $p = \|\mathbf{p}\|$.

Our paper is organized as follows. In Section 2, we summarize previous results on the case when only the magnetic field is present. This allows us to introduce Delaunay variables and the method of averaging, and illustrate them in a relatively simple situation.

In Section 3, we consider the case when only an electric field is present, which is integrable [R63]. We introduce another set of action–angle variables ("electric action–angle variables") based on parabolic variables, which are better adapted to perturbation theory [B27]. We then derive (new) transformation formulas from electric action–angle variables to the geometrically more transparent Delaunay variables.

With these tools and sets of coordinates in mind, we finally turn to the crossed-fields Hamiltonian (1) in Section 4. We start by considering the two limiting cases $B \ll F$ and $F \ll B$, which involve three distinct time scales, and can thus be analysed by a second averaging. We then study the dynamics in the plane perpendicular to $\mathbf{B}$ for general values of the fields. We conclude by an overview of the general structure of the phase space of the averaged Hamiltonian.

2   The Quadratic Zeeman Effect (or DKP)

We start by considering Hamiltonian (1) in the case $F = 0$. If we take the z-axis along the magnetic field $\mathbf{B}$, (1) can be written as

$$H = \frac{1}{2}p^2 - \frac{1}{r} + \frac{B}{2}L_z + \frac{B^2}{8}(x^2 + y^2). \tag{2}$$

Although the equations of motion are easily written down, it is difficult to understand the qualitative properties of dynamics in cartesian coordinates. We will therefore take advantage of the fact that for small B, (2) is a small perturbation of the integrable Kepler problem, for which action–angle variables are known explicitly. By writing the Hamiltonian (2) in these variables, we can separate slow and fast components of the motion. The qualitative dynamics can then be further analysed by using the method of averaging.

2.1   Delaunay variables

We start by considering the Kepler Hamiltonian

$$H = \frac{1}{2}p^2 - \frac{1}{r}. \tag{3}$$

Besides the energy H, it admits as constants of motion the angular momentum $\mathbf{L}$ and the Runge-Lenz vector

$$\mathbf{A} = \frac{\mathbf{r}}{r} + \mathbf{L} \wedge \mathbf{p}. \tag{4}$$

If $H < 0$, the motion takes place in a plane perpendicular to $\mathbf{L}$, on an ellipse of eccentricity $e = \|\mathbf{A}\|$ and major axis parallel to $\mathbf{A}$ and of length $2a = -1/H$.

Action–angle variables taking these properties into account are well known in celestial
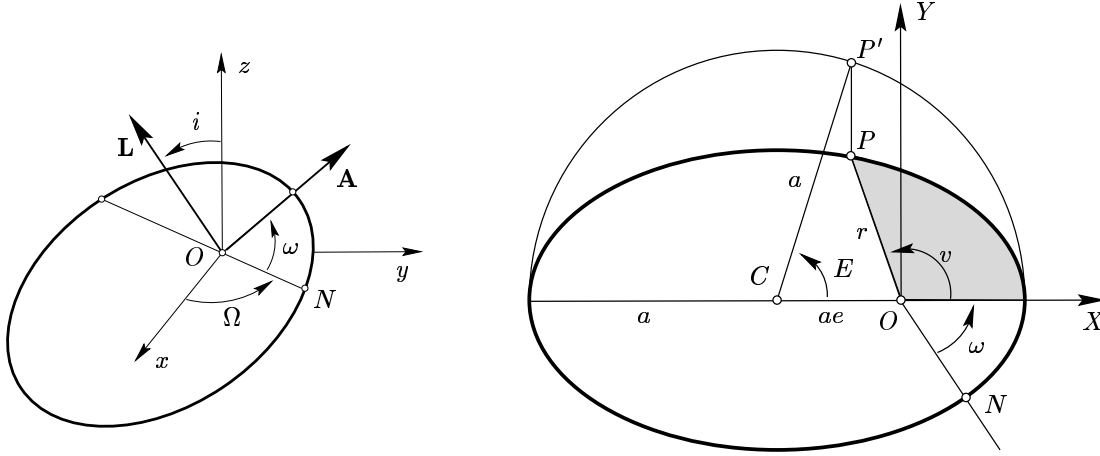
FIGURE 1. Definition of Delaunay variables. The angles Ω, i and ω determine the position of the Kepler ellipse in space. The line of nodes ON is the intersection of the plane of the ellipse with the xy-plane. The shaded area is proportional to the mean anomaly M. The true anomaly v and eccentric anomaly E are auxiliary quantities, allowing to relate the (X, Y)-coordinates of the planet P with M.

mechanics, where they are called *Delaunay variables*. The action variables are given by[1]

$$
\begin{aligned}
\Lambda &= \sqrt{a} \\
G &= \sqrt{a}\sqrt{1-e^2} = \|\mathbf{L}\| \\
K &= \sqrt{a}\sqrt{1-e^2}\,\cos i = L_z,
\end{aligned}
\tag{5}
$$

where the inclination $i \in [0, \pi]$ is the angle between $\mathbf{L}$ and the z-axis. These variables are defined on the domain $|K| \leqslant G \leqslant \Lambda$.

The corresponding angle variables are defined in the following way. The intersection between the plane of the orbit and the xy-plane is called *line of nodes*. The angle Ω between line of nodes and x-axis is called *longitude of nodes* and is conjugated to K; the angle ω between major axis of the Kepler ellipse and line of nodes is called *argument of perihelion* and is conjugated to G; the *mean anomaly* M, which is conjugated to Λ, is proportional to the area swept on the ellipse, according to Kepler's second law.

In order to compute M, we introduce orthogonal coordinates (X, Y), where X is attached to the major axis of the ellipse. The *true anomaly* v and the *eccentric anomaly* E are auxiliary quantities defined by the relations

$$
\begin{aligned}
X &= r\cos v = a(\cos E - e) \\
Y &= r\sin v = a\sqrt{1-e^2}\,\sin E,
\end{aligned}
\tag{6}
$$

see Fig. 1. By trigonometry one can show that M and E are related by *Kepler's equation*

$$
M = E - e\sin E,
\tag{7}
$$

which implies in particular that

$$
\frac{\mathrm{d}M}{\mathrm{d}E} = 1 - e\cos E = \frac{r}{a}.
\tag{8}
$$

---

[1]We use the letters G and K in order to distinguish the action variables from their physical meaning. In celestial mechanics, one usually denotes L_z by H instead of K, but we prefer the latter notation in order to avoid confusion with the Hamiltonian.

The transition from Delaunay variables to cartesian coordinates is done in the following way. Given the actions (5), we can compute

$$a = \Lambda^2, \qquad e^2 = 1 - \frac{G^2}{\Lambda^2}, \qquad \cos i = \frac{K}{G}. \tag{9}$$

We can then determine X, Y and the conjugated momenta

$$P_X = -\frac{1}{\sqrt{a}} \frac{\sin E}{1 - e \cos E}$$

$$P_Y = \frac{1}{\sqrt{a}} \frac{\sqrt{1 - e^2} \cos E}{1 - e \cos E}. \tag{10}$$

The cartesian coordinates are then given by the relations

$$\begin{pmatrix} x & p_x \\ y & p_y \\ z & p_z \end{pmatrix} = \mathcal{R}_z(\Omega) \mathcal{R}_x(i) \mathcal{R}_z(\omega) \begin{pmatrix} X & P_X \\ Y & P_Y \\ 0 & 0 \end{pmatrix}, \tag{11}$$

where $\mathcal{R}_x$ and $\mathcal{R}_z$ describe rotations around the x- and z-axis, given by

$$\mathcal{R}_x(i) = \begin{pmatrix} 1 & 0 & 0 \\ 0 & \cos i & -\sin i \\ 0 & \sin i & \cos i \end{pmatrix}, \qquad \mathcal{R}_z(\omega) = \begin{pmatrix} \cos \omega & -\sin \omega & 0 \\ \sin \omega & \cos \omega & 0 \\ 0 & 0 & 1 \end{pmatrix}. \tag{12}$$

It is then straightforward to show that the Hamiltonian (3) takes the form

$$H = -\frac{1}{2\Lambda^2}, \tag{13}$$

and thus the equations of motion are given by

$$\begin{aligned} \dot{\Lambda} &= 0 & \dot{M} &= \frac{1}{\Lambda^3} \\ \dot{G} &= 0 & \dot{\omega} &= 0 \\ \dot{K} &= 0 & \dot{\Omega} &= 0. \end{aligned} \tag{14}$$

Besides the actions Λ, G, K, the two angles ω and Ω are also constants, which reflects the high degeneracy of the hydrogen atom. Equation (13) also gives a physical interpretation of Λ as a function of the energy. In quantum mechanics, Λ corresponds to the principal quantum number.

Let us now return to the Zeeman effect. The Hamiltonian (2) can be expressed in Delaunay variables as

$$H = -\frac{1}{2\Lambda^2} + \frac{B}{2} K + B^2 H_1(\Lambda, G, K; M, \omega)$$

$$H_1 = \tfrac{1}{16} r^2 \left[1 + \cos^2 i + \sin^2 i \cos(2\omega + 2v) \right], \tag{15}$$

where r, $\sin i$ and v can be expressed in terms of Delaunay variables using (6), (8) and (9). The equations of motion take the form

$$\begin{aligned} \dot{\Lambda} &= B^2 \{\Lambda; H_1\} & \dot{M} &= \frac{1}{\Lambda^3} + B^2 \{M; H_1\} \\ \dot{G} &= B^2 \{G; H_1\} & \dot{\omega} &= \qquad B^2 \{\omega; H_1\} \\ \dot{K} &= 0 & \dot{\Omega} &= \frac{B}{2} + B^2 \{\Omega; H_1\}, \end{aligned} \tag{16}$$

where the Poisson bracket is defined by

$$\{f;g\} = \frac{\partial f}{\partial M}\frac{\partial g}{\partial \Lambda} - \frac{\partial f}{\partial \Lambda}\frac{\partial G}{\partial M} + \frac{\partial f}{\partial \omega}\frac{\partial g}{\partial G} - \frac{\partial f}{\partial G}\frac{\partial g}{\partial \omega} + \frac{\partial f}{\partial \Omega}\frac{\partial g}{\partial K} - \frac{\partial f}{\partial K}\frac{\partial g}{\partial \Omega}. \tag{17}$$

We discuss the computation of these Poisson brackets in Appendix B (see in particular Table 3).

To first order in B, (16) describes the Larmor precession of the ellipse. Since the Hamiltonian does not depend on Ω, $K = L_z$ is a constant of the motion and (16) is in effect a two-degrees-of-freedom system. For small B, M is a fast variable, while Λ, G and ω are slow ones. The motion can thus be imagined as a fast motion of the electron along a slowly "breathing" and rotating ellipse. The dynamics can be visualized by a Poincaré map, taking for instance a section at constant M, and plotting the value of G and ω at each intersection [DKN83].

2.2   Averaging

To analyse the motion of (16) for small B, one can use the fact that M is the only fast variable, so that the dynamics of the slow variables will be essentially determined by the average effect of M during one period.

With any given function f of the Delaunay variables, let us associate its average

$$\langle f\rangle_\Lambda(G,K;\omega,\Omega) = \frac{1}{2\pi}\int_0^{2\pi} f(\Lambda,G,K;M,\omega,\Omega)\,\mathrm{d}M. \tag{18}$$

The averaged Hamiltonian $\langle H\rangle_\Lambda$ generates the canonical equations

$$\dot\Lambda = 0 \qquad\qquad\qquad \dot M = \frac{1}{\Lambda^3} + B^2\{M;\langle H_1\rangle_\Lambda\}$$

$$\dot G = B^2\{G;\langle H_1\rangle_\Lambda\} \qquad\qquad \dot\omega = \qquad B^2\{\omega;\langle H_1\rangle_\Lambda\} \tag{19}$$

$$\dot K = 0 \qquad\qquad\qquad \dot\Omega = \frac{B}{2} + B^2\{\Omega;\langle H_1\rangle_\Lambda\}.$$

Since $\langle H_1\rangle_\Lambda$ does not depend on M and Ω, $\langle H\rangle_\Lambda$ is in effect a one-degree-of-freedom Hamiltonian, depending on K and Λ as on parameters.

A standard result from averaging theory (see Appendix A) states that the equations (19) are a good approximation of the equations (16), in the sense that

- orbits of (19) and (16) with the same initial condition differ by a term of order B^2 during a time of order $1/B^2$;
- to each nondegenerate equilibrium of (19), there corresponds a periodic orbit of (16), at a distance of order B^2 of the equilibrium, and which has the same stability if the equilibrium is hyperbolic.

Averages over M can be computed quite easily by the formula

$$\langle f\rangle_\Lambda = \frac{1}{2\pi}\int_0^{2\pi} f(M)\frac{\mathrm{d}M}{\mathrm{d}E}\,\mathrm{d}E = \frac{1}{2\pi}\int_0^{2\pi} f(M(E))(1 - e\cos E)\,\mathrm{d}E. \tag{20}$$

Some useful averages are given in Table 1. The averaged Hamiltonian can be written in the form [CDMW87]

$$\langle H_1\rangle_\Lambda = \tfrac{1}{16}\Lambda^4\Big[(1+\cos^2 i)(1+\tfrac{3}{2}e^2) + \tfrac{5}{2}e^2\sin^2 i\cos 2\omega\Big], \tag{21}$$

f	$\langle f \rangle_\Lambda$	f	$\langle f \rangle_\Lambda$
X	$-\frac{3}{2}ae$	X^2	$a^2(\frac{1}{2} + 2e^2)$
Y	0	Y^2	$a^2(\frac{1}{2} - \frac{1}{2}e^2)$
r	$a(1 + \frac{1}{2}e^2)$	r^2	$a^2(1 + \frac{3}{2}e^2)$
z	$-\frac{3}{2}ae\sin i \sin \omega$	z^2	$a^2 \sin^2 i\left[\frac{1}{2} + \frac{1}{4}e^2(3 - 5\cos 2\omega)\right]$

TABLE 1. Some important quantities and their averages over the fast variable M.

from which we deduce the relevant equations of motion

$$\dot{G} = \frac{5}{16}B^2\Lambda^4 e^2 \sin i \sin 2\omega$$
$$\dot{\omega} = \frac{1}{16}B^2\frac{\Lambda^4}{G}\left[3(e^2 - 1) - 5\cos^2 i + 5(e^2 - \sin^2 i)\cos 2\omega\right]. \tag{22}$$

The system can now be studied by analysing the orbits of (22) or, equivalently, the level lines of the function (21) in the (ω, G)-plane [DKN83]. Doing this, one finds that the vector field has two elliptic equilibrium points located at

$$\omega = \frac{\pi}{2}, \frac{3\pi}{2}, \qquad G^2 = \sqrt{5}|K|\Lambda, \tag{23}$$

which exist if $|K| < \Lambda/\sqrt{5}$.

The vector field behaves in a singular way at the boundaries $G = |K|$ and $G = \Lambda$ of the domain. These singularities have been explained by Coffey and coworkers [CDMW87], who showed that the phase space has the topology of a sphere. The line $G = \Lambda$, $\omega \in [0, 2\pi)$ has to be contracted into the north pole of the sphere, corresponding to $e = 0$ and thus to circular motion; indeed, in this case the perihelion, and hence its argument ω, is undefined. The line $G = |K|$, $\omega \in [0, 2\pi)$ has to be contracted into the south pole of the sphere, corresponding to $i = 0$ and thus to equatorial motion; in that case, the sum $\Omega + \omega$ is sufficient to specify the position of the ellipse.

To account for the spherical topology of phase space, [CDMW87] have introduced the variables

$$\xi_1 = G\Lambda e \sin i \, \cos \omega$$
$$\xi_2 = G\Lambda e \sin i \, \sin \omega \tag{24}$$
$$\xi_3 = G^2 - \tfrac{1}{2}(\Lambda^2 + K^2),$$

which belong to the sphere

$$\xi_1^2 + \xi_2^2 + \xi_3^2 = \left(\frac{\Lambda^2 - K^2}{2}\right)^2. \tag{25}$$

Using the fact that $\langle H_1 \rangle_\Lambda$ can be put into the form

$$\langle H_1 \rangle_\Lambda = \frac{\Lambda^4}{16}\left[1 + \cos^2 i + 3e^2 + \frac{\xi_1^2 - 4\xi_2^2}{\Lambda^2 G^2}\right], \tag{26}$$
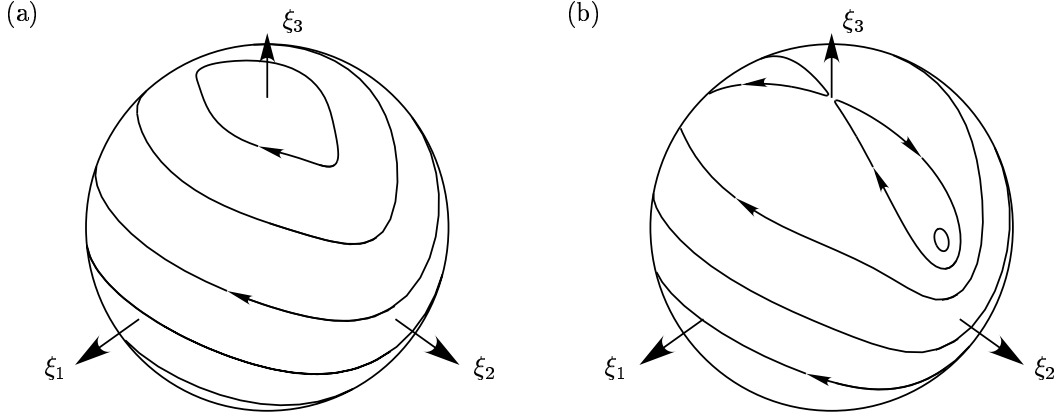
7

FIGURE 2. Phase portraits of the averaged Hamiltonian (20) on the sphere $\xi_1^2 + \xi_2^2 + \xi_3^2 = \left(\frac{1}{2}(\Lambda^2 - K^2)\right)^2$, (a) for $|K| > \Lambda/\sqrt{5}$ and (b) for $|K| < \Lambda/\sqrt{5}$. The north pole corresponds to circular C-orbits, the south pole (not shown) to equatorial B-orbits, which are elliptic in both cases. In the second case, two additional periodic orbits (the Z-orbits) appear in the plane $\xi_1 = 0$.

and the Poisson brackets in Table 4 of Appendix B, they derive the equations of motion

$$\dot{\xi}_1 = \frac{\Lambda^4}{8G}\,\xi_2\Big[\frac{5\xi_1^2}{\Lambda^2 G^2} - 1 + e^2 + 5\cos^2 i\Big]$$

$$\dot{\xi}_2 = \frac{\Lambda^4}{8G}\,\xi_1\Big[\frac{5\xi_2^2}{\Lambda^2 G^2} - 4(1 - e^2)\Big] \tag{27}$$

$$\dot{\xi}_3 = \frac{5\Lambda^2}{4G}\,\xi_1\xi_2.$$

In these variables, the poles have become equilibrium points around which the flow is nonsingular, so that their stability can be easily determined. Depending on the relative value of the constants of motion Λ and K, there are two qualitatively different phase portraits (Fig. 2):

1. If $|K| > \Lambda/\sqrt{5}$, both poles are elliptic, and there are no other equilibrium points. All other orbits rotate around the sphere with $\dot{\omega} < 0$ (Fig. 2a).
2. If $|K| < \Lambda/\sqrt{5}$, the south pole is still elliptic, but the north pole has become hyperbolic, and the new elliptic equilibria (23) have appeared in a pitchfork bifurcation. Two homoclinic orbits of the north pole separate orbits rotating around each of the three elliptic equilibria (Fig. 2b).

The averaging theorem shows that to each of the four possible equilibrium points of (27), there corresponds a periodic orbit of the exact system (16) (see also Appendix B). For further reference, let us call B-orbits the equatorial orbits (which lie in the plane perpendicular to $\mathbf{B}$), C-orbits the circular ones, and Z-orbits those corresponding to the nontrivial equilibrium (23). One further expects that the periodic orbits of (27) approximate either quasiperiodic KAM-type orbits of (16), or "soft" chaotic components associated with resonances. More prominent chaotic components are expected near the homoclinic orbits of the north pole.

In other works [HRW89], orbits are sometimes represented in cylindric coordinates

(ρ, ϕ, z). They can be deduced from Delaunay variables by the relations

$$z = r \sin i \sin(\omega + v)$$
$$\rho = r\sqrt{1 - \sin^2 i \sin^2(\omega + v)}. \tag{28}$$

The different periodic orbits can thus be parametrized either by the true anomaly v or by the eccentric anomaly E as

$$
\begin{array}{lll}
\text{C-orbits} & z = \Lambda\sqrt{\Lambda^2 - K^2}\,\sin v & \rho = \Lambda\sqrt{\Lambda^2 \cos^2 v + K^2 \sin^2 v} \\[4pt]
\text{B-orbits} & z = 0 & \rho = \Lambda(\Lambda - \sqrt{\Lambda^2 - K^2}\cos E) \\[4pt]
\text{Z-orbits} & z = \Lambda^2 \sin i\,(\cos E - e) & \rho = \Lambda^2\sqrt{(1 - e\cos E)^2 - \sin^2 i\,(\cos E - e)^2},
\end{array}
\tag{29}
$$

where $\sin^2 i = 1 - |K|/\sqrt{5}\Lambda$ and $e^2 = 1 - \sqrt{5}|K|/\Lambda$ in the last case. The C-, B- and Z-orbits are labelled, respectively, C, I_1 and I_∞ in [HRW89].

3 The Stark effect

We consider now the Hamiltonian (1) in the case $B = 0$. If we choose the z-axis along the electric field $\mathbf{F}$, it can be written as

$$H = \frac{1}{2}p^2 - \frac{1}{r} + Fz. \tag{30}$$

Besides the energy and the z-component of the angular momentum, this system has a third constant of the motion and is thus integrable. Indeed, as shown by [R63], the generalization of the Runge-Lenz vector (4),

$$\mathbf{C} = \mathbf{A} - \frac{1}{2}(\mathbf{r} \wedge \mathbf{F}) \wedge \mathbf{r} \tag{31}$$

satisfies the equation of motion

$$\dot{\mathbf{C}} = \frac{3}{2}\mathbf{L} \wedge \mathbf{F}, \tag{32}$$

and thus $C_z = \mathbf{C} \cdot \mathbf{F}$ is constant.

We will start, in Section 3.1, by analysing the system in Delaunay variables, in particular in its averaged form, in order to get a feeling for the geometry of the orbits. In Section 3.2, we present another description of the system, based on parabolic variables, which allows to construct action–angle variables taking the constant C_z into account. Though they are better suited for perturbation theory, these action–angle variables have a less obvious geometric interpretation than Delaunay variables. This is why we establish the transformation formulas between both sets of variables in Section 3.3, in the limit $F \to 0$.

3.1 Delaunay variables

In Delaunay variables, the Hamiltonian (30) takes the form

$$H = -\frac{1}{2\Lambda^2} + FH_2(\Lambda, G, K; M, \omega),$$
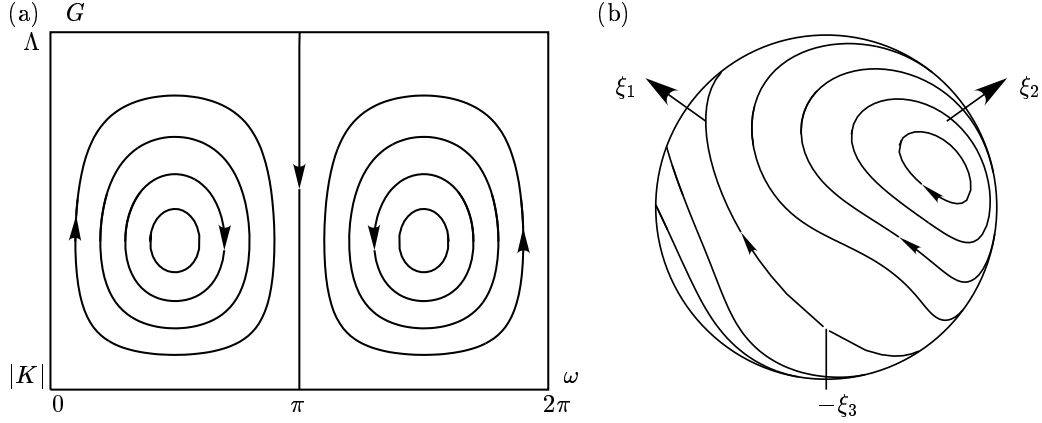$$H_2 = r \sin i\,\sin(\omega + v), \tag{33}$$

FIGURE 3. Phase portraits of the averaged Hamiltonian (36) (a) in the (ω, G)-plane and (b) on the sphere $\xi_1^2 + \xi_2^2 + \xi_3^2 = \left(\frac{1}{2}(\Lambda^2 - K^2)\right)^2$, seen from below the south pole. The elliptic points at $\omega = \frac{\pi}{2}, \frac{3\pi}{2}$ correspond to periodic S-orbits of the Stark Hamiltonian.

and the equations of motion have the structure

$$\dot{\Lambda} = F\{\Lambda; H_2\} \qquad\qquad \dot{M} = \frac{1}{\Lambda^3} + F\{M; H_2\}$$

$$\dot{G} = F\{G; H_2\} \qquad\qquad \dot{\omega} = \qquad F\{\omega; H_2\} \qquad\qquad (34)$$

$$\dot{K} = 0 \qquad\qquad\qquad \dot{\Omega} = \qquad F\{\Omega; H_2\}.$$

The constants of motion are H, K and

$$C_z = -e \sin i \, \sin \omega - \frac{1}{2} F r^2 \left[1 - \sin^2 i \sin^2(\omega + v)\right]. \qquad (35)$$

In order to understand the geometry of the orbits for small F, we may analyse the averaged Hamiltonian

$$\langle H \rangle_\Lambda = \frac{1}{2\Lambda^2} - \frac{3}{2} F a e \sin i \, \sin \omega. \qquad (36)$$

The relevant equations of motion of this one-degree-of-freedom system are

$$\begin{aligned} \dot{G} &= \tfrac{3}{2} F \Lambda^2 e \sin i \, \cos \omega, \\ \dot{\omega} &= \tfrac{3}{2} F \frac{G^4 - K^2 \Lambda^2}{G^3 e \sin i} \sin \omega. \end{aligned} \qquad (37)$$

We observe the existence of a pair of elliptic stationary points at $\omega = \frac{\pi}{2}, \frac{3\pi}{2}$ and $G^2 = |K|\Lambda$, which implies $e = \sin i = \sqrt{1 - |K|/\Lambda}$ (Fig. 3a). When $F = 0$, the constant of motion C_z reaches its extremal values $\pm(1 - K/|\Lambda|)$ on these points. We will call S-orbits the associated periodic orbits of the Stark Hamiltonian. In order to analyse the motion at the boundaries of phase space, we use again the variables (24). Since the averaged Hamiltonian can be written as

$$\langle H_2 \rangle_\Lambda = -\frac{3}{2} \frac{\Lambda}{G} \xi_2, \qquad (38)$$
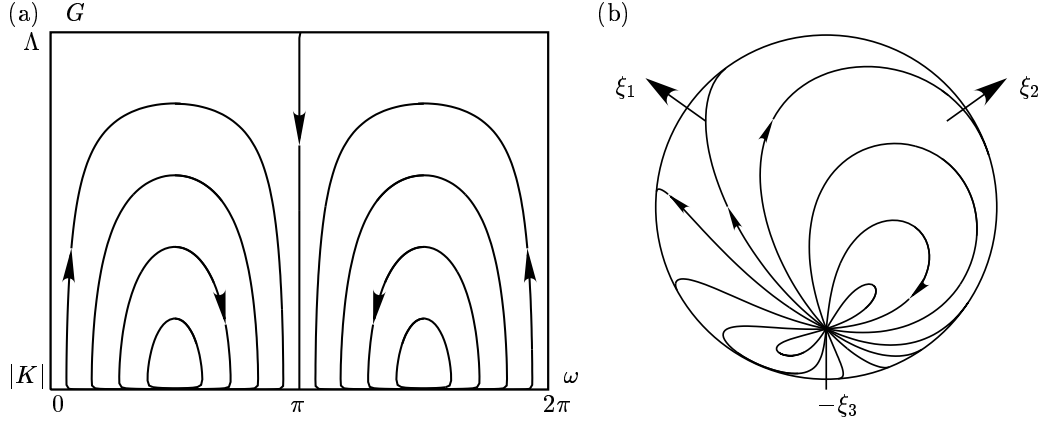
10

FIGURE 4. Same as Fig. 3, but for $K = 0$.

they evolve according to

$$\dot{\xi}_1 = \tfrac{3}{2}F\frac{\Lambda}{G^2}\left[-\xi_2^2 - (\Lambda^2 + K^2 + 2\xi_3)\xi_3\right]$$
$$\dot{\xi}_2 = \tfrac{3}{2}F\frac{\Lambda}{G^2}\xi_1\xi_2 \qquad\qquad (39)$$
$$\dot{\xi}_3 = 3F\Lambda\xi_1.$$

This shows that there are no other equilibrium points than the two elliptic ones, since the flow is nonsingular at the poles (Fig. 3b).

Besides the periodic orbits corresponding to the elliptic equilibrium points of (37), the system displays quasiperiodic orbits for which both ω and G oscillate. There is a particular orbit following the meridian $\xi_2 = 0$ of the sphere, for which the Kepler ellipse oscillates between a circular and an equatorial one, while its major axis is always perpendicular to $\mathbf{F}$. Note that the case $K = 0$ is special, since the elliptic points merge at the south pole. All orbits then go through the south pole, where the eccentricity vanishes, which means that the electron approaches the nucleus arbitrarily closely (Fig. 4).

3.2 Parabolic and electric action–angle variables

The separability of the Stark Hamiltonian in parabolic variables was already known to Max Born [B27] from the earlier works of P.S. Epstein [E16] and K. Schwarzschild [Schw16]. Parabolic variables $(P_\xi, P_\eta, P_\varphi; \xi, \eta, \varphi)$ are defined by

$$x = \xi\eta\cos\varphi \qquad\qquad p_x = \frac{\eta P_\xi + \xi P_\eta}{\xi^2 + \eta^2}\cos\varphi - \frac{P_\varphi}{\xi\eta}\sin\varphi$$

$$y = \xi\eta\sin\varphi \qquad\qquad p_y = \frac{\eta P_\xi + \xi P_\eta}{\xi^2 + \eta^2}\sin\varphi + \frac{P_\varphi}{\xi\eta}\cos\varphi \qquad\qquad (40)$$

$$z = \frac{1}{2}(\xi^2 - \eta^2) \qquad\qquad p_z = \frac{\xi P_\xi - \eta P_\eta}{\xi^2 + \eta^2},$$

where $P_\varphi = L_z = K$ is the z-component of the angular momentum.

In these variables, the Hamiltonian takes the form

$$H = \frac{1}{\xi^2 + \eta^2}\left[\frac{1}{2}P_\xi^2 + \frac{K^2}{2\xi^2} + F\xi^4 + \frac{1}{2}P_\eta^2 + \frac{K^2}{2\eta^2} - F\eta^4 - 2\right]. \qquad\qquad (41)$$
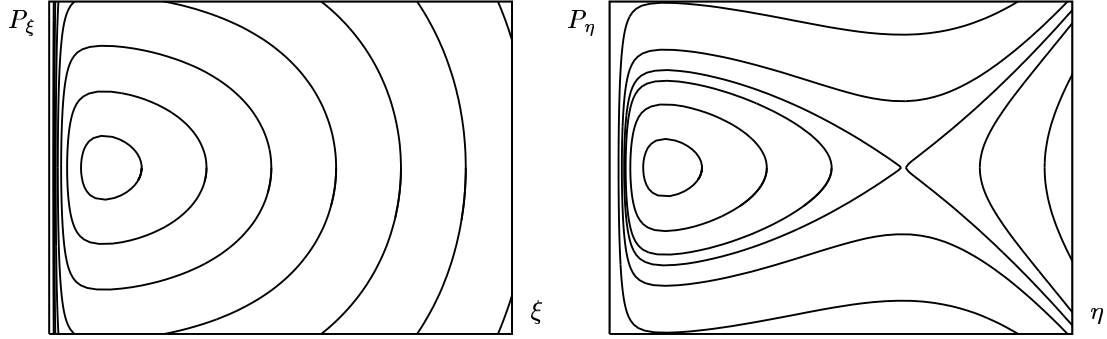
11

FIGURE 5. Level lines of the constants of motion α_1 and α_2 for $H = 1$, $K = \frac{1}{2}$ and $F = 0.05$. In contrast to ξ, η may have an unbounded motion. However, the saddle point is located quite far away from the origin, at $\eta^2 = \mathcal{O}(F^{-1})$.

There are four constants of motion H, α_1, α_2, K, related by

$$\alpha_1 = \frac{1}{2}P_\xi^2 + \frac{K^2}{2\xi^2} - \xi^2 H + F\xi^4$$

$$\alpha_2 = \frac{1}{2}P_\eta^2 + \frac{K^2}{2\eta^2} - \eta^2 H - F\eta^4 \tag{42}$$

$$\alpha_1 + \alpha_2 = 2.$$

If one scales time by a factor $\xi^2 + \eta^2$, (41) is seen to describe the motion of two decoupled "oscillators". In fact, the constant α_1 is of the form $\frac{1}{2}P_\xi^2 + V_1(\xi)$, where $V_1(\xi) \to \infty$ in both limits $\xi \to 0$ and $\xi \to \infty$ when $F > 0$. Thus the motion of ξ is always bounded. By contrast, $\alpha_2 = \frac{1}{2}P_\eta^2 + V_2(\eta)$, where $V_2(\eta) \to -\infty$ for $\eta \to \infty$. Thus the level sets of α_2 may be unbounded for large values of η^2 or α_2 (of order F^{-1}), corresponding to ionization (Fig. 5). The following discussion is limited to the bounded motion of η, which exists for small F. In that case, action–angle variables can be constructed.

Action variables related to the constants α_1 and α_2 are defined by

$$J_\xi = \frac{1}{2\pi} \oint \sqrt{2H + \frac{2\alpha_1}{\xi^2} - \frac{K^2}{\xi^4} - 2F\xi^2}\, \xi\, \mathrm{d}\xi$$

$$J_\eta = \frac{1}{2\pi} \oint \sqrt{2H + \frac{2\alpha_2}{\eta^2} - \frac{K^2}{\eta^4} + 2F\eta^2}\, \eta\, \mathrm{d}\eta, \tag{43}$$

where the integrals are over bounded level sets of α_1 and α_2, respectively. In the case $F = 0$, they can be computed explicitly [B27]:

$$J_\xi = \frac{1}{2}\left[-K + \frac{\alpha_1}{\sqrt{-2H}}\right], \qquad J_\eta = \frac{1}{2}\left[-K + \frac{\alpha_2}{\sqrt{-2H}}\right]. \tag{44}$$

From this we deduce that

$$H = -\frac{1}{2(J_\xi + J_\eta + K)^2}, \qquad \alpha_{1,2} = \frac{2J_{\xi,\eta} + K}{J_\xi + J_\eta + K}, \tag{45}$$

which shows, by comparison with (13), that $J_\xi + J_\eta + K = \Lambda$ is nothing but the first Delaunay action. Moreover, one finds that the constant of motion C_z reduces to

$$A_z = 1 - \alpha_2 = \alpha_1 - 1 = \frac{J_\xi - J_\eta}{\Lambda}, \tag{46}$$

12

which suggests to introduce the action $J_{\mathrm{e}} = J_\eta - J_\xi$. In quantum mechanics, J_{e} corresponds to the electric quantum number. For further reference, let us call $(\Lambda, J_{\mathrm{e}}, K)$ the *electric action variables*. As we have seen that $|A_z| \leqslant 1 - |K|/\Lambda$ for $F = 0$, they vary on the square domain

$$-(\Lambda - |K|) \leqslant J_{\mathrm{e}} \leqslant \Lambda - |K|. \tag{47}$$

For $F > 0$, we need to know the expression of the Hamiltonian in action variables. This can be done perturbatively [DK83] with the result

$$H(\Lambda, J_{\mathrm{e}}, K) = -\frac{1}{2\Lambda^2} - 3F\Lambda J_{\mathrm{e}} - \frac{1}{4}F^2\Lambda^4(17\Lambda^2 - 3J_{\mathrm{e}}^2 - 9K^2) + \mathcal{O}(F^3). \tag{48}$$

The associated canonical equations are

$$\dot{\Lambda} = 0 \qquad \dot{w}_\Lambda = \frac{1}{\Lambda^3} - 3FJ_{\mathrm{e}} - \tfrac{3}{2}F^2\Lambda^3(17\Lambda^2 - 2J_{\mathrm{e}}^2 - 6K^2) + \mathcal{O}(F^3)$$

$$\dot{J}_{\mathrm{e}} = 0 \qquad \dot{w}_{\mathrm{e}} = \qquad -3F\Lambda + \tfrac{3}{2}F^2\Lambda^4 J_{\mathrm{e}} + \mathcal{O}(F^3) \tag{49}$$

$$\dot{K} = 0 \qquad \dot{w}_K = \qquad\qquad \tfrac{9}{2}F^2\Lambda^4 K + \mathcal{O}(F^3),$$

where w_Λ, w_{e} and w_K (the *electric angle variables*) are conjugated to Λ, J_{e} and K respectively. In the case $F = 0$, these equations are equivalent to the equations (14) in Delaunay variables. The electric field suppresses the degeneracies of the Kepler problem, and introduces different time scales for the various angles.

In order to compute the electric angle variables, we need to parametrize the level curves of α_1 and α_2. For $F = 0$, using (45) the first equation of (42) can be written as

$$P_\xi^2 + \frac{(\xi^2 - \xi_+^2)(\xi^2 - \xi_-^2)}{\Lambda^2\xi^2} = 0, \tag{50}$$

where $\xi_\pm^2 = a_1 \pm b_1$ are extremal values of ξ^2 with

$$a_1 = \Lambda(2J_\xi + K), \qquad b_1 = 2\Lambda\sqrt{J_\xi(J_\xi + K)}. \tag{51}$$

Similarly, η^2 can vary between $a_2 - b_2$ and $a_2 + b_2$. In terms of the electric actions $(\Lambda, J_{\mathrm{e}}, K)$, these limits are given by

$$a_1 = \Lambda(\Lambda - J_{\mathrm{e}}) \qquad\qquad b_1 = \Lambda\sqrt{(\Lambda - J_{\mathrm{e}})^2 - K^2}$$

$$a_2 = \Lambda(\Lambda + J_{\mathrm{e}}) \qquad\qquad b_2 = \Lambda\sqrt{(\Lambda + J_{\mathrm{e}})^2 - K^2}. \tag{52}$$

Relation (50) is the equation of an ellipse in the $(\xi^2, \Lambda\xi P_\xi)$-plane, which suggests to parametrize the level sets by

$$\xi = \sqrt{a_1 - b_1\cos\psi} \qquad\qquad \eta = \sqrt{a_2 - b_2\cos\chi}$$

$$P_\xi = \frac{b_1\sin\psi}{\Lambda\xi} \qquad\qquad P_\eta = \frac{b_2\sin\chi}{\Lambda\eta}, \tag{53}$$

where ψ and χ are auxiliary angles, playing a similar role as the eccentric anomaly E in the case of Delaunay variables. If we introduce the action

$$S = \int^\xi P_\xi\,\mathrm{d}\xi' + \int^\eta P_\eta\,\mathrm{d}\eta' + K\varphi, \tag{54}$$

the angles conjugated to (J_ξ, J_η, K) are given by the formulas

$$w_\xi = \frac{\partial S}{\partial J_\xi}, \qquad w_\eta = \frac{\partial S}{\partial J_\eta}, \qquad w_\varphi = \frac{\partial S}{\partial K}, \tag{55}$$

and the angles conjugated to (Λ, J_e, K) are then obtained by the linear transformation

$$w_\Lambda = \tfrac{1}{2}(w_\xi + w_\eta), \qquad w_e = \tfrac{1}{2}(w_\eta - w_\xi), \qquad w_K = w_\varphi - w_\Lambda. \tag{56}$$

With the parametrization (53), the derivatives (55) take a simple form [B27], and the final result is

$$\begin{aligned} w_\Lambda &= \frac{\psi + \chi}{2} - \frac{1}{2\Lambda^2}(b_1 \sin \psi + b_2 \sin \chi) \\ w_e &= \frac{\chi - \psi}{2} \\ w_K &= \varphi - \rho_1(\psi) - \rho_2(\chi), \end{aligned} \tag{57}$$

where

$$\rho_j(\theta) = \frac{K\Lambda}{2} \int_0^\theta \frac{\mathrm{d}\theta'}{a_j - b_j \cos \theta'}, \qquad j = 1, 2. \tag{58}$$

Using the fact that $a_1^2 - b_1^2 = K^2 \Lambda^2$, this expression can be written as

$$\rho_j(\theta) = \mathrm{sign}(K) \, \mathrm{atan}\left[\sqrt{\frac{a_j + b_j}{a_j - b_j}} \tan \frac{\theta}{2}\right] \qquad \text{for } -\pi \leqslant \theta \leqslant \pi, \tag{59}$$

and can be continued to arbitrary θ by the rule $\rho_j(\theta + k2\pi) = \rho_j(\theta) + k\pi$ for $k \in \mathbb{Z}$. This implies that for *all* θ, we have

$$\cos \rho_j(\theta) = \frac{\sqrt{a_j - b_j}}{\sqrt{a_j - b_j \cos \theta}} \cos \frac{\theta}{2}, \qquad \sin \rho_j(\theta) = \mathrm{sign}\, K \frac{\sqrt{a_j + b_j}}{\sqrt{a_j - b_j \cos \theta}} \sin \frac{\theta}{2}. \tag{60}$$

Note in particular that the transformation $w_e \mapsto w_e + \pi$, $w_\Lambda \mapsto w_\Lambda + \pi$ corresponds to keeping ψ fixed and increasing χ by 2π. Hence it leaves all parabolic variables fixed, except φ which is increased by π. In other words, this transformation describes a rotation of angle π around the z-axis.

The relations (57) are valid for $F = 0$. Higher order expressions in F of the angle variables can be computed perturbatively, see Appendix C.

3.3 Correspondence between electric action–angle and Delaunay variables

We now establish transformation formulas between electric action–angle variables and Delaunay variables in the case $F = 0$. In the two-dimensional case, corresponding to $K = 0$, this issue has been addressed in [DW91], in connection with Lissajous variables.

The most important relations can be obtained by averaging over the fast variable w_Λ. In view of (57), the averaging operation can be written as

$$\langle f(\psi, \chi) \rangle_\Lambda = \frac{1}{2\pi} \int_0^{2\pi} f(\psi, \psi + 2w_e)\left[1 - \frac{b_1 \cos \psi + b_2 \cos(\psi + 2w_e)}{2\Lambda^2}\right] \mathrm{d}\psi. \tag{61}$$

14

f	$\langle f \rangle_\Lambda$	f	$\langle f \rangle_\Lambda$
$\cos\psi$	$-\frac{b_1}{4\Lambda^2} - \frac{b_2}{4\Lambda^2}\cos 2w_{\rm e}$	$\cos\chi$	$-\frac{b_1}{4\Lambda^2}\cos 2w_{\rm e} - \frac{b_2}{4\Lambda^2}$
$\sin\psi$	$\frac{b_2}{4\Lambda^2}\sin 2w_{\rm e}$	$\sin\chi$	$-\frac{b_1}{4\Lambda^2}\sin 2w_{\rm e}$
$\cos^2\psi$	$\frac{1}{2}$	$\cos^2\chi$	$\frac{1}{2}$
$\cos\psi\cos\chi$	$\frac{1}{2}\cos 2w_{\rm e}$	$\cos\psi\sin\chi$	$-\frac{1}{2}\sin 2w_{\rm e}$
$\sin\psi\sin\chi$	$\frac{1}{2}\cos 2w_{\rm e}$	$\sin\psi\cos\chi$	$\frac{1}{2}\sin 2w_{\rm e}$

TABLE 2. The averages over the fast variable w_Λ of some important quantities. Using (53) they can be used to compute averages of some polynomials in ξ^2 and η^2.

A few useful averages are given in Table 2. We can thus easily compute the averages

$$
\begin{aligned}
\langle z \rangle_\Lambda &= \frac{1}{2}\langle \xi^2 - \eta^2 \rangle_\Lambda = -\tfrac{3}{2}\Lambda J_{\rm e} \\
\langle r \rangle_\Lambda &= \frac{1}{2}\langle \xi^2 + \eta^2 \rangle_\Lambda = \Lambda^2\Big[1 + \frac{1}{8\Lambda^4}(b_1^2 + b_2^2 + 2b_1 b_2 \cos 2w_{\rm e})\Big].
\end{aligned}
\tag{62}
$$

Comparison with the corresponding averages over M (Table 1) gives us the relations

$$
J_{\rm e} = \Lambda e \sin i \sin\omega,
\tag{63}
$$

$$
e^2 = \frac{1}{4\Lambda^4}\big(b_1^2 + b_2^2 + 2b_1 b_2 \cos 2w_{\rm e}\big).
\tag{64}
$$

This last relation allows to compute G and i. It has a nice geometric interpretation: the maximal value of e^2 (hence the minimal value of G) is attained for $w_{\rm e} = 0$ and π, while the minimal value of e^2 is reached for $w_{\rm e} = \frac{\pi}{2}$ and $\frac{3\pi}{2}$. According to Fig. 3a, these values of $w_{\rm e}$ correspond to $\omega = \frac{\pi}{2}\operatorname{sign} J_{\rm e}$. From the fact that $\dot{w}_{\rm e} < 0$ for $F > 0$, we infer that

$$
\operatorname{sign}(\cos\omega) = -\operatorname{sign}(\sin 2w_{\rm e}).
\tag{65}
$$

The relations (63), (64) and (65) determine the transformation $(G,\omega) \mapsto (J_{\rm e}, w_{\rm e})$ up to a phase π of $w_{\rm e}$, which depends on Ω.

It remains to establish relations between the angles (w_Λ, w_K) and (M, Ω). Since $\dot{w}_\Lambda = \dot{M}$ for $F = 0$, the difference $w_\Lambda - M$ does not depend on M. From (53) we deduce that in electric action–angle variables,

$$
r = \Lambda^2\Big[1 - \frac{1}{2\Lambda^2}(b_1\cos\psi + b_2\cos\chi)\Big] = \Lambda^2\Big(\frac{\partial w_\Lambda}{\partial\psi} + \frac{\partial w_\Lambda}{\partial\chi}\Big).
\tag{66}
$$

Comparison with (8) yields the equalities

$$
e\cos E = \frac{1}{2\Lambda^2}(b_1\cos\psi + b_2\cos\chi),
\tag{67}
$$

and, using $\dot{w}_\Lambda = \dot{M}$,

$$
\frac{\mathrm{d}}{\mathrm{d}E} = \frac{\mathrm{d}M}{\mathrm{d}E}\frac{\mathrm{d}}{\mathrm{d}M} = \Big(\frac{\partial w_\Lambda}{\partial\psi} + \frac{\partial w_\Lambda}{\partial\chi}\Big)\frac{\mathrm{d}}{\mathrm{d}w_\Lambda} = \frac{\partial}{\partial\psi} + \frac{\partial}{\partial\chi}.
\tag{68}
$$

15

Applied to (67), this also gives

$$e \sin E = \frac{1}{2\Lambda^2}(b_1 \sin \psi + b_2 \sin \chi). \tag{69}$$

In particular, when $M = 0$ we have $E = 0$ and thus by (57) $w_\Lambda = \frac{\psi + \chi}{2}$. Inserting the relations $\psi = w_\Lambda - w_e$ and $\chi = w_\Lambda + w_e$ into (67) and (69), we can solve for $\cos w_\Lambda$ and $\sin w_\Lambda$ with the result, for general values of M,

$$\cos(w_\Lambda - M) = \frac{2\Lambda^2 e}{b_1 + b_2} \cos w_e, \qquad \sin(w_\Lambda - M) = \frac{2\Lambda^2 e}{b_2 - b_1} \sin w_e. \tag{70}$$

Relation (68) also implies that

$$\psi - E = w_\Lambda - w_e - M, \qquad \chi - E = w_\Lambda + w_e - M. \tag{71}$$

Determining w_K is a bit more delicate. We will use the fact that in Delaunay variables, the x-component of the angular momentum is

$$L_x = \sqrt{G^2 - K^2} \sin \Omega, \tag{72}$$

while in parabolic variables, we have from (40)

$$L_x = \frac{1}{2}(\eta P_\xi - \xi P_\eta) \sin \varphi - \frac{1}{2} \frac{K}{\xi \eta}(\xi^2 - \eta^2) \cos \varphi. \tag{73}$$

Being independent of M, L_x also has to be independent of w_Λ. We may thus evaluate (73) in the case $\psi = 0$, $\chi = 2w_e$. Then (53) reduces to

$$\xi = \sqrt{a_1 - b_1}, \qquad \eta = \sqrt{a_2 - b_2 \cos 2w_e}, \qquad P_\xi = 0, \qquad P_\eta = \frac{b_2 \sin 2w_e}{\Lambda \eta}, \tag{74}$$

and (57) implies $\varphi = w_K + \rho_2$, where

$$\cos \rho_2 = \frac{\sqrt{a_2 - b_2}}{\eta} \cos w_e, \qquad \sin \rho_2 = \mathrm{sign}(K)\frac{\sqrt{a_2 + b_2}}{\eta} \sin w_e. \tag{75}$$

Inserting (74) and (75) into (73), we obtain

$$L_x = L_1 \cos w_K + L_2 \sin w_K, \tag{76}$$

where

$$\begin{aligned}
\frac{L_1}{\cos w_e} &= -\frac{1}{2\Lambda\xi\eta^2}\left[2\,\mathrm{sign}(K)\xi^2\sqrt{a_2 + b_2}\,b_2 \sin^2 w_e + K\Lambda(\xi^2 - \eta^2)\sqrt{a_2 - b_2}\right] \\
&= \frac{1}{2}K\sqrt{\frac{a_2 - b_2}{a_1 - b_1}} - \frac{\xi}{2\Lambda\eta^2\sqrt{a_2 - b_2}}\left[K\Lambda(a_2 - b_2) + 2\,\mathrm{sign}(K)b_2\sqrt{a_2^2 - b_2^2}\sin^2 w_e\right] \\
&= \frac{1}{2}K\left[\sqrt{\frac{a_2 - b_2}{a_1 - b_1}} - \sqrt{\frac{a_1 - b_1}{a_2 - b_2}}\right],
\end{aligned} \tag{77}$$

where we have used the relation $\sqrt{a_2^2 - b_2^2} = |K|\Lambda$. The term L_2 can be evaluated in a similar way. We obtain the following, relatively compact expression of L_x in electric action–angle variables:

$$L_x = Y_1(\Lambda, J_e, K) \cos w_e \cos w_K + Y_2(\Lambda, J_e, K) \sin w_e \sin w_K, \tag{78}$$

16

where we have introduced the notations

$$Y_1(\Lambda, J_\mathrm{e}, K) = \frac{1}{2} K \left[\sqrt{\frac{a_2 - b_2}{a_1 - b_1}} - \sqrt{\frac{a_1 - b_1}{a_2 - b_2}} \right]$$

$$Y_2(\Lambda, J_\mathrm{e}, K) = -\frac{1}{2} |K| \left[\sqrt{\frac{a_2 + b_2}{a_1 - b_1}} - \sqrt{\frac{a_1 - b_1}{a_2 + b_2}} \right]. \tag{79}$$

Comparison with (72) gives the desired relation between w_K and Ω:

$$\sqrt{G^2 - K^2} \sin(\Omega - w_K) = Y_1(\Lambda, J_\mathrm{e}, K) \cos w_\mathrm{e}$$

$$\sqrt{G^2 - K^2} \cos(\Omega - w_K) = Y_2(\Lambda, J_\mathrm{e}, K) \sin w_\mathrm{e}. \tag{80}$$

We point out that despite the absolute value, the expressions (79) are regular at $K = 0$ and admit the Taylor series

$$Y_1(\Lambda, J_\mathrm{e}, K) = -K \frac{J_\mathrm{e}}{\sqrt{\Lambda^2 - J_\mathrm{e}^2}} + K^3 \frac{\Lambda^2 J_\mathrm{e}}{2(\Lambda^2 - J_\mathrm{e}^2)^{5/2}} + \mathcal{O}(K^5)$$

$$Y_2(\Lambda, J_\mathrm{e}, K) = -\sqrt{\Lambda^2 - J_\mathrm{e}^2} + K^2 \frac{\Lambda^2}{2(\Lambda^2 - J_\mathrm{e}^2)^{3/2}} + \mathcal{O}(K^4). \tag{81}$$

4 The crossed-fields problem

We now consider the full crossed-fields Hamiltonian (1), in the case $0 < B, F \ll 1$. First, we have to choose a system of coordinates. Both sets of action–angle variables that we have used so far are defined with respect to a privileged direction (the z-axis). Depending on the regime we consider, it will be most convenient to choose this direction along the electric or along the magnetic field. In the first case, the Hamiltonian takes the form

$$H = \frac{1}{2} p^2 - \frac{1}{r} + Fz + \frac{1}{2} B L_x + \frac{1}{8} B^2 (y^2 + z^2). \tag{82}$$

To account for the second case, we also introduce coordinates $(x', y', z') = (z, y, x)$. In Section 4.1, we consider the case $B \ll F$, which is a small perturbation of the integrable Stark effect, and thus particularly well suited to perturbation theory. The case $F \ll B$ is considered in Section 4.2. The orbits contained in the plane perpendicular to $\mathbf{B}$ exist for all values of the fields. We analyse them in Section 4.3. Other periodic orbits and the general structure of phase space are discussed in Section 4.4.

4.1 The case $B \ll F$

When the magnetic field acts as a small perturbation of the Stark Hamiltonian, it is best to use the electric action–angle variables introduced in Section 3.2. The Hamiltonian can be written as

$$H = H_0(\Lambda, J_\mathrm{e}, K; F) + B H_1(\Lambda, J_\mathrm{e}, K; w_\mathrm{e}, w_K; F)$$
$$+ B^2 H_2(\Lambda, J_\mathrm{e}, K; w_\Lambda, w_\mathrm{e}, w_K; F), \tag{83}$$

where $H_0 = -\frac{1}{2\Lambda^2} - 3F\Lambda J_\mathrm{e} + F^2 h_2(\Lambda, J_\mathrm{e}, K; F)$ is the Stark Hamiltonian (48), $H_1 = \frac{1}{2} L_x$ has been computed in (78), and $H_2 = \frac{1}{8}(y^2 + z^2)$. The equations of motion thus have the

17

structure

$$\dot{\Lambda} = \mathcal{O}(B^2) \qquad\qquad \dot{w_\Lambda} = \frac{1}{\Lambda^3} - 3FJ_e + \mathcal{O}(F^2) + \mathcal{O}(B)$$

$$\dot{J_e} = \mathcal{O}(B) \qquad\qquad \dot{w_e} = \qquad -3F\Lambda + \mathcal{O}(F^2) + \mathcal{O}(B) \qquad (84)$$

$$\dot{K} = \mathcal{O}(B) \qquad\qquad \dot{w_K} = \qquad\qquad \mathcal{O}(F^2) + \mathcal{O}(B)$$

We can again average over the fast variable w_Λ, using the rule (61). Since L_x does not depend on w_Λ, H_1 is already in averaged form. The equations of the averaged system are thus given by

$$\dot{J_e} = \qquad\qquad B\{J_e; H_1\} + B^2\{J_e; \langle H_2\rangle_\Lambda\}$$
$$\dot{K} = \qquad\qquad B\{K; H_1\} + B^2\{K; \langle H_2\rangle_\Lambda\}$$

$$(85)$$

$$\dot{w_e} = -3F\Lambda + F^2\{w_e; h_2\} + B\{w_e; H_1\} + B^2\{w_e; \langle H_2\rangle_\Lambda\}$$
$$\dot{w_K} = \qquad F^2\{w_K; h_2\} + B\{w_K; H_1\} + B^2\{w_K; \langle H_2\rangle_\Lambda\}$$

Since we assume that $B \ll F$, w_e evolves on a faster time scale than w_K. We may thus further approximate the dynamics by averaging over w_e, that is, we define the double average

$$\langle\langle f\rangle\rangle_{\Lambda, J_e}(K; w_K) = \frac{1}{4\pi^2} \int_0^{2\pi} \int_0^{2\pi} f(\Lambda, J_e, K; w_\Lambda, w_e, w_K)\, \mathrm{d}w_\Lambda\, \mathrm{d}w_e. \qquad (86)$$

The doubly-averaged Hamiltonian $\langle\langle H\rangle\rangle_{\Lambda, J_e}$ has one degree of freedom and is thus integrable. Let us now compute various averages, at lowest order in F. In order to compute $\langle H_2\rangle_\Lambda$, we need to evaluate the average of

$$y^2 + z^2 = \xi^2\eta^2 \sin^2\varphi + \tfrac{1}{4}(\xi^4 + \eta^4 - 2\xi^2\eta^2). \qquad (87)$$

Using the expressions in Table 2, the second term is easily averaged. To average the first term, we use the fact that with (57) and (60), $\xi\eta\sin\varphi$ can be written as a polynomial in $\sqrt{a_1 \pm b_1}$, $\sqrt{a_2 \pm b_2}$, and sines and cosines of w_K, $\frac{\psi}{2}$ and $\frac{\chi}{2}$. The final result after simplification is

$$\langle y^2 + z^2\rangle_\Lambda = \tfrac{1}{2}\Lambda^2(2\Lambda^2 + 3J_e^2 - K^2) - \tfrac{3}{4}b_1 b_2 \cos 2w_K$$
$$+ \tfrac{1}{4}b_1 b_2 \cos 2w_e - \tfrac{1}{2}\Lambda^2(\Lambda^2 - J_e^2 - K^2)\cos 2w_e \cos 2w_K \qquad (88)$$
$$- \Lambda^2 J_e K \sin 2w_e \sin 2w_K + \mathcal{O}(F).$$

Computation of the doubly-averaged Hamiltonian is now easy. From (78) and (88) we obtain

$$\langle\langle L_x\rangle\rangle_{\Lambda, J_e} = \mathcal{O}(F)$$
$$(89)$$
$$\langle\langle y^2 + z^2\rangle\rangle_{\Lambda. J_e} = \tfrac{1}{2}\Lambda^2(2\Lambda^2 + 3J_e^2 - K^2) - \tfrac{3}{4}b_1 b_2 \cos 2w_K + \mathcal{O}(F).$$

In fact, equation (122) in Appendix C shows that also at order F (and probably at all higher orders), the transformation $w_e \mapsto w_e + \pi$, $w_\Lambda \mapsto w_\Lambda + \pi$ describes a rotation of angle π around the z-axis. Since this rotation changes L_x into $-L_x$, we conclude that
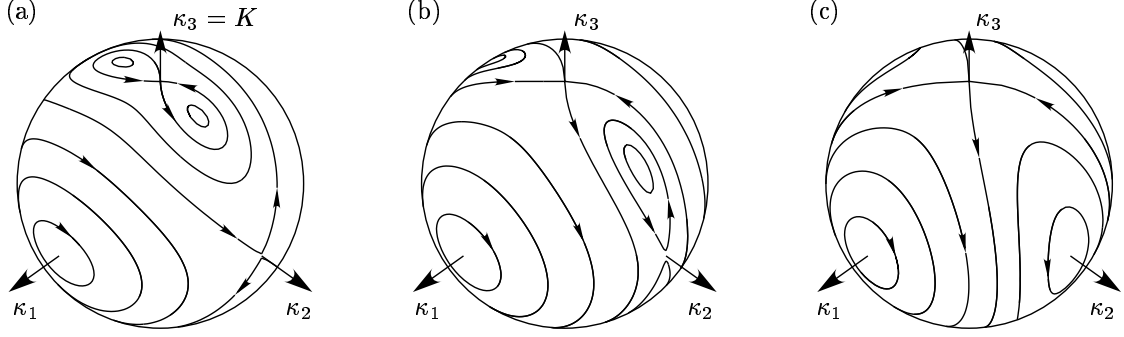
FIGURE 6. Phase portraits of the doubly-averaged system (90) on the sphere $\kappa_1^2 + \kappa_2^2 + \kappa_3^2 = (\Lambda - |J_e|)^2$, (a) for $0 < B < B_2$, where B_2 is given by (95), (b) for $B_2 < B < B_1$, given by (93), and (c) for $B > B_1$. The poles (the intersection of the sphere with the κ_3-axis) correspond to the S-orbits present in the Stark effect. The intersections of the sphere with the κ_1- and κ_2-axis correspond respectively to the BF-orbits, lying in the plane defined by $\mathbf{B}$ and $\mathbf{F}$, and the B-orbits, lying in the plane perpendicular to $\mathbf{B}$.

$\langle\langle L_x \rangle\rangle_{\Lambda, J_e} = \mathcal{O}(F^2)$. Discarding irrelevant constant terms, the doubly-averaged Hamiltonian can be written as

$$\langle\langle H \rangle\rangle_{\Lambda, J_e} = \tfrac{9}{4} F^2 \Lambda^4 K^2 - \tfrac{1}{16} B^2 \left[\Lambda^2 K^2 + \tfrac{3}{2} b_1 b_2 \cos 2w_K \right] + \mathcal{O}(F^3, BF^2, B^2 F), \qquad (90)$$

where b_1 and b_2 are given in (52) and the remainder denotes a sum of terms of order F^3, BF^2 and B^2F. Besides Λ and J_e, (90) is a third adiabatic invariant of the crossed-fields Hamiltonian in the case $B \ll F \ll 1$. Up to the remainders, the equations of motion have the form

$$\dot{K} = -\frac{3}{16} B^2 b_1 b_2 \sin 2w_K$$
$$\dot{w}_K = \frac{9}{2} F^2 \Lambda^4 K - \frac{1}{8} B^2 \Lambda^2 K \left[1 - \frac{3}{2} \frac{\Lambda^2}{b_1 b_2} (\Lambda^2 + J_e^2 - K^2) \cos 2w_K \right]. \qquad (91)$$

We should also examine the topology of phase space. From (47), we deduce that in the limit $F \to 0$, K varies between $-(\Lambda - |J_e|)$ and $\Lambda - |J_e|$. If, say, $J_e \geqslant 0$ and $K = \Lambda - J_e$, we have $b_1 = 0$ and the angle ψ is undefined. Since $\rho_1(\psi) = \frac{\psi}{2}$ in this case, we obtain from (53) and (57) that the quantities $w_\Lambda + w_K$ and $w_\Lambda + w_e$ are sufficient to determine the state of the system completely. We conclude that in the averaged phase space, the variables w_K and w_e are irrelevant when $|K| = \Lambda - |J_e|$, and thus we have again a spherical topology. The sphere can be parametrized by

$$(\kappa_1, \kappa_2, \kappa_3) = (\sqrt{(\Lambda - |J_e|)^2 - K^2} \cos w_K, \sqrt{(\Lambda - |J_e|)^2 - K^2} \sin w_K, K). \qquad (92)$$

We now analyse the structure of phase space for increasing B. When $B = 0$, the orbits of (91) follow the parallels of the sphere. The poles and all points of the equator $K = 0$ are fixed points. For slightly positive B, a resonance of order 2 is created: only the points $w_K = 0, \frac{\pi}{2}, \pi, \frac{3\pi}{2}$ of the equator remain fixed. A straightforward stability analysis shows that the points $(w_K, K) = (0, 0)$ and $(\pi, 0)$ are always elliptic, while the points $(\frac{\pi}{2}, 0)$ and $(\frac{3\pi}{2}, 0)$ are hyperbolic for

$$B \leqslant B_1 = 6\sqrt{2} F \Lambda \sqrt{\frac{\Lambda^2 - J_e^2}{5\Lambda^2 + J_e^2}}, \qquad (93)$$

19

and elliptic for $B \geqslant B_1$. If $J_e \neq 0$, there is another pair of equilibrium points, located at $w_K = \frac{\pi}{2}, \frac{3\pi}{2}$ and $K = K_\star$, given by the condition

$$\left(6\frac{F}{B}\Lambda\right)^2 = 1 + \frac{3}{2}\frac{\Lambda^2 + J_e^2 - K_\star^2}{\sqrt{[(\Lambda - J_e)^2 - K_\star^2][(\Lambda + J_e)^2 - K_\star^2]}}. \tag{94}$$

These orbits are created in a pitchfork bifurcation at the poles at $B = 0$ (Fig. 6a), move to the equator as B increases (Fig. 6b), and disappear in another pitchfork bifurcation at $B = B_1$ (Fig. 6c). It is easy to see that there must be a global bifurcation involving a saddle connection between these values. It is given by the condition

$$\langle\langle H \rangle\rangle_{\Lambda, J_e}(\tfrac{\pi}{2}, 0) = \langle\langle H \rangle\rangle_{\Lambda, J_e}(w_K, \Lambda - |J_e|) \quad \Rightarrow \quad B = B_2 = 6\sqrt{2}F\Lambda\sqrt{\frac{\Lambda - |J_e|}{5\Lambda + |J_e|}}. \tag{95}$$

At $B = B_2$, the poles of the sphere are connected with the points $(\frac{\pi}{2}, 0)$ and $(\frac{3\pi}{2}, 0)$ on the equator by heteroclinic orbits. In the case $J_e = 0$, all these bifurcations collapse.

Our analysis of the doubly-averaged Hamiltonian (90) has thus revealed a rather rich structure of phase space. We point out that only the first case, depicted in Fig. 6a, is compatible with the hypothesis $B \ll F$, which is necessary for the doubly-averaged system to be a reliable approximation. We will see in the next sections, however, that the picture given in Fig. 6 also contains some truth in the other parameter ranges (see Fig. 12).

We conclude that for $B \ll F$, the structure of phase space is determined by four types of orbits:

1. The poles of the sphere (92) correspond to the fixed points of the averaged Stark Hamiltonian, and thus to the periodic S-orbits of the original (unaveraged) Hamiltonian (83). They are unstable unless $J_e = 0$.

2. The points $K = 0$, $w_K = \frac{\pi}{2}$ or $\frac{3\pi}{2}$, which are hyperbolic for small B, correspond to $\Omega = \frac{\pi}{2}$ or $\frac{3\pi}{2}$ in Delaunay variables, and hence describe the B-orbits, which lie in the plane perpendicular to $\mathbf{B}$. In the singly-averaged system, they appear as periodic orbits, following a curve of constant J_e. Since $K = 0$, all these curves agglomerate at the points $G = 0$ and $\omega = \frac{\pi}{2}$ or $\frac{3\pi}{2}$ (see Fig. 4). In the original system, the orbits can be interpreted as a fast rotation along a slowly "breathing" Kepler ellipse, reaching periodically the eccentricity $e = 1$, where the electron approaches the nucleus indefinitely closely.

3. The points $K = 0$, $w_K = 0$ or π, which are elliptic, correspond to $\Omega = 0$ or π, and thus describe orbits in the plane of $\mathbf{F}$ and $\mathbf{B}$. As in the previous case, they evolve on a level curve of J_e containing a point with zero angular momentum. We will call them the BF-orbits.

4. Finally, the four points $(\pm\frac{\pi}{2}, \pm K_\star)$ describe more complicated orbits, which are stable and provide a connection between S-orbits and B-orbits. For small B, they are close to the S-orbits. Let us thus call them SB-orbits.

4.2 The case $F \ll B$

When perturbing the Zeeman effect, it seems more appropriate to use coordinates (x', y', z') in which the magnetic field is vertical. The Hamiltonian takes the form

$$H = \frac{1}{2}p^2 - \frac{1}{r} + \frac{1}{2}BL_{z'} + \frac{1}{8}B^2(x'^2 + y'^2) + Fx'. \tag{96}$$

We will denote by $(\Lambda', G', K'; M', \omega', \Omega')$ the associated Delaunay variables. The transformation between these Delaunay variables and those defined with respect to $(x, y, z) = (z', y', x')$ can be derived by expressing $\mathbf{L}$ and z in both sets of variables. The result is

$$
\begin{aligned}
\Lambda &= \Lambda' & G &= G' \\
K &= \sqrt{G'^2 - K'^2} \sin \Omega' & \sin^2 i &= \cos^2 \Omega' + \cos^2 i' \sin^2 \Omega' \\
\cos \Omega &= \frac{\sqrt{G'^2 - K'^2} \cos \Omega'}{\sqrt{G'^2 \cos^2 \Omega' + K'^2 \sin^2 \Omega'}} & \cos \omega &= -\frac{\sin \omega' \cos \Omega' + \cos i' \cos \omega' \sin \Omega'}{\sin i} \\
\sin \Omega &= \frac{K'}{\sqrt{G'^2 \cos^2 \Omega' + K'^2 \sin^2 \Omega'}} & \sin \omega &= \frac{\cos \omega' \cos \Omega' - \cos i' \sin \omega' \sin \Omega'}{\sin i}.
\end{aligned}
\tag{97}
$$

The averaged Hamiltonian over M' takes the form

$$
\begin{aligned}
\langle H \rangle_\Lambda &= -\frac{1}{2\Lambda^2} + \frac{B}{2} K + B^2 \langle H_1 \rangle_\Lambda (G', K'; \omega') + F \langle H_2 \rangle_\Lambda (G', K'; \omega', \Omega') \\
\langle H_1 \rangle_\Lambda &= \frac{1}{16} \left[(1 + \cos^2 i')(1 + \tfrac{3}{2} e'^2) + \tfrac{5}{2} e'^2 \sin^2 i' \cos 2\omega' \right] \\
\langle H_2 \rangle_\Lambda &= -\tfrac{3}{2} \Lambda^2 e' (\cos \omega' \cos \Omega' - \sin \omega' \sin \Omega' \cos i').
\end{aligned}
\tag{98}
$$

It generates the equations of motion

$$
\dot{K}' = F\{K'; \langle H_2 \rangle_\Lambda\} \quad \dot{\Omega}' = \frac{B}{2} + B^2\{\Omega'; \langle H_1 \rangle_\Lambda\} + F\{\Omega'; \langle H_2 \rangle_\Lambda\}
$$

$$
\dot{G}' = B^2\{G'; \langle H_1 \rangle_\Lambda\} + F\{G'; \langle H_2 \rangle_\Lambda\} \quad \dot{\omega}' = B^2\{\omega'; \langle H_1 \rangle_\Lambda\} + F\{\omega'; \langle H_2 \rangle_\Lambda\}. \tag{99}
$$

We observe that for $F \ll B$, Ω' evolves on a faster time scale that ω', and the dynamics can be further approximated by averaging the Hamiltonian over Ω'. Note, however, that the average of $\langle H_2 \rangle_\Lambda$ over Ω' vanishes, while $\langle H_1 \rangle_\Lambda$ does not depend on Ω'. The twice averaged Hamiltonian is thus strictly equivalent to the averaged Zeeman Hamiltonian (21). This means that to lowest order in perturbation theory, the electric field does not influence the phase portrait of the Zeeman effect, which has one of the two behaviours indicated in Fig. 2. The phase space is thus organized around three types of periodic orbits:

1. a stable B-orbit at $K' = G'$, located in the plane perpendicular to $\mathbf{B}$;
2. a circular C-orbit, stable for large K' and unstable for small K';
3. and a pair of stable Z-orbits, existing only for small K', with a major axis perpendicular to the line of nodes.

These orbits will experience deformations of magnitude $\mathcal{O}(F^2)$ when $F > 0$.

4.3 The B-orbits

Let us now examine the most important periodic orbits for general (small) values of F and B. A special role is played by the orbits in the plane perpendicular to $\mathbf{B}$, which we called B-orbits. Their existence can already be seen on the original Hamiltonian (82), which leaves the plane $x = 0$ invariant. The Hamiltonian restricted to this plane has two degrees of freedom, its averaged version will thus have one degree of freedom. Hence *all* orbits starting in that plane will look periodic in the averaged system, but may correspond to quasiperiodic or soft chaotic components of the original Hamiltonian.

In the two previous sections, we have found that the B-orbits are hyperbolic in the limit $B \to 0$ and elliptic in the limit $F \to 0$. Hence there must be at least one bifurcation value
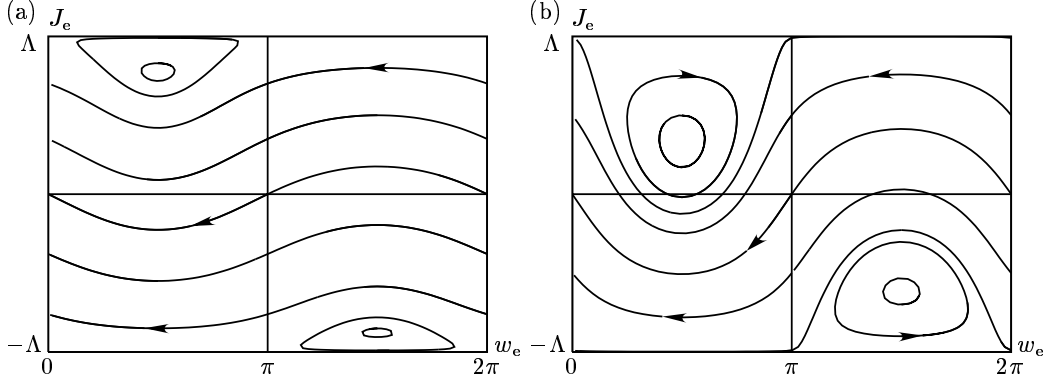
FIGURE 7. Orbits of the averaged Hamiltonian (100) restricted to the plane perpendicular to **B**. (a) shows a case with $B < F$, and (b) shows a case with $F < B$. There are two types of orbits, those which cross the lines $w_e = 0$ and π, and those which oscillate around $w_e = \frac{\pi}{2}$ and $\frac{3\pi}{2}$. The second type will not appear on a Poincaré section at $w_e = 0$.

between these limits. The twice averaged Hamiltonian in electric action–angle variables (90) suggested that this transition should be given by the condition (93), which is, however, not in the range where (90) can be expected to be a good approximation. We will now examine this question in more detail with the once averaged Hamiltonian.

Using the expansion (81) of L_x for small K, it is easy to compute the equations of motion (85) of the singly-averaged Hamiltonian in electric action–angle variables. One can then check that both $\dot{w}_K$ and $\dot{K}$ vanish for $K = 0$ and $\cos w_K = 0$, which confirms the invariance of the subspace of B-orbits. The motion in this subspace is determined by the one-degree-of-freedom Hamiltonian

$$
\begin{aligned}
\langle H \rangle_\Lambda(J_e, 0; w_e, \tfrac{\pi}{2}) = & - 3F\Lambda J_e + \tfrac{3}{4}F^2\Lambda^4 J_e^2 + \mathcal{O}(F^3) \\
& - \tfrac{1}{2}B\sqrt{\Lambda^2 - J_e^2}\sin w_e + \tfrac{3}{32}B^2\Lambda^2\big[\Lambda^2 + J_e^2 + (\Lambda^2 - J_e^2)\cos 2w_e\big] \\
& + \mathcal{O}(BF).
\end{aligned}
\tag{100}
$$

Up to the remainders, its equations of motion are given by

$$
\begin{aligned}
\dot{J}_e &= \frac{1}{2}B\sqrt{\Lambda^2 - J_e^2}\cos w_e + \frac{3}{16}B^2\Lambda^2(\Lambda^2 - J_e^2)\sin 2w_e \\
\dot{w}_e &= -3F\Lambda + \frac{3}{2}F^2\Lambda^4 J_e + \frac{1}{2}B\frac{J_e}{\sqrt{\Lambda^2 - J_e^2}}\sin w_e + \frac{3}{8}B^2\Lambda^2 J_e \sin^2 w_e.
\end{aligned}
\tag{101}
$$

This system admits two elliptic equilibria located at $w_e = \frac{\pi}{2}$ and $\frac{3\pi}{2}$ and

$$
J_e \simeq \pm\Lambda\Big[1 + \Big(\frac{B}{6F\Lambda}\Big)^2\Big]^{-1/2}.
\tag{102}
$$

These points move from the boundaries $|J_e| = \Lambda$ to $J_e = 0$ as $\frac{B}{F}$ increases from 0 to ∞. The orbits of (101) are shown in Fig. 7. They are of two types:

1. the orbits which cross the lines $w_e = 0$ and π, and for which w_e is monotonous;
2. the orbits which oscillate around $w_e = \frac{\pi}{2}$ and $\frac{3\pi}{2}$ without reaching $w_e = 0$ or π.

There is no separatrix between both types of orbits, the flow being regular when expressed in the right variables (the boundaries $|J_e| = \Lambda$ should again be contracted into the poles of a sphere, since they correspond to the periodic S-orbits of the Stark effect). Still, there
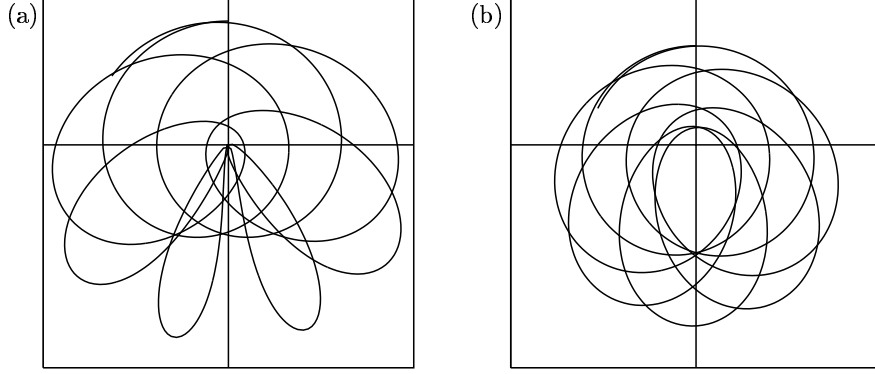
FIGURE 8. The two types of equatorial orbits: (a) singular orbits, which periodically reach an eccentricity $e = 1$, and (b), regular orbits which are bounded away from $e = 1$. The electric field is vertical, while the magnetic field points out of the plane. One can identify the fast motion along a Kepler ellipse, the parameters of which evolve approximately on a level curve of Fig. 3 in the regular case, and of Fig. 4 in the singular case. These orbits are not periodic in general, as can be seen on the pictures.

is an important qualitative difference between both types of orbits. Indeed, by (64), the values $w_e = 0, \pi$ are the only ones that lead to an eccentricity $e = 1$ when $K = 0$, and thus imply a close encounter with the nucleus. Hence, the first type of orbits will contain cusps (*singular* orbits, Fig. 8a), and the second will not (*regular* orbits, Fig. 8b). The boundary between both types of orbits, when starting on the line $w_e = \frac{\pi}{2}$, is given by the condition

$$\langle H \rangle_\Lambda(\Lambda, 0; \tfrac{\pi}{2}, \tfrac{\pi}{2}) = \langle H \rangle_\Lambda(J_e, 0; \tfrac{\pi}{2}, \tfrac{\pi}{2}) \quad \Rightarrow \quad B \simeq 6F\Lambda\sqrt{\frac{\Lambda - J_e}{\Lambda + J_e}}. \tag{103}$$

We will now examine the stability of the B-orbits in the 4-dimensional phase space of the averaged Hamiltonian. To do this, we first need to compute the derivatives

$$\begin{aligned}
\frac{\partial \dot{w}_K}{\partial w_K}\Big|_{\frac{\pi}{2},0} &= \frac{1}{2}B\frac{J_e}{\sqrt{\Lambda^2 - J_e^2}}\cos w_e + \frac{1}{4}B^2\Lambda^2 J_e \sin 2w_e = -\frac{\partial \dot{K}}{\partial K}\Big|_{\frac{\pi}{2},0} \\
\frac{\partial \dot{w}_K}{\partial K}\Big|_{\frac{\pi}{2},0} &= \frac{9}{2}F^2\Lambda^4 + \frac{B}{2}\frac{\Lambda^2}{(\Lambda^2 - J_e^2)^{3/2}}\sin w_e \\
&\quad - \frac{1}{16}B^2\frac{\Lambda^2}{\Lambda^2 - J_e^2}\big[5\Lambda^2 + J_e^2 + (3\Lambda^2 - J_e^2)\cos 2w_e\big] \\
\frac{\partial \dot{K}}{\partial w_K}\Big|_{\frac{\pi}{2},0} &= -\frac{1}{2}B\sqrt{\Lambda^2 - J_e^2}\sin w_e + \frac{1}{8}B^2\Lambda^2(\Lambda^2 - J_e^2)\big[3 + 2\cos 2w_e\big].
\end{aligned} \tag{104}$$

In order to determine the stability of a B-orbit, we have to find the multipliers of the variational equation

$$\dot{z} = A(w_e, J_e)z, \tag{105}$$

integrated over a solution of the system (101), where $z^T = (w_K - \frac{\pi}{2}, 0)$, and A is the matrix with entries given by (104).

Two limiting cases can be studied analytically. When $B \to 0$, A can be replaced by its average over the fast variable w_e, and we obtain again the condition (93), which tells us that only orbits with $\Lambda^2 - J_e^2 = \mathcal{O}(B^2/F^2)$ are elliptic. The other case is that of the
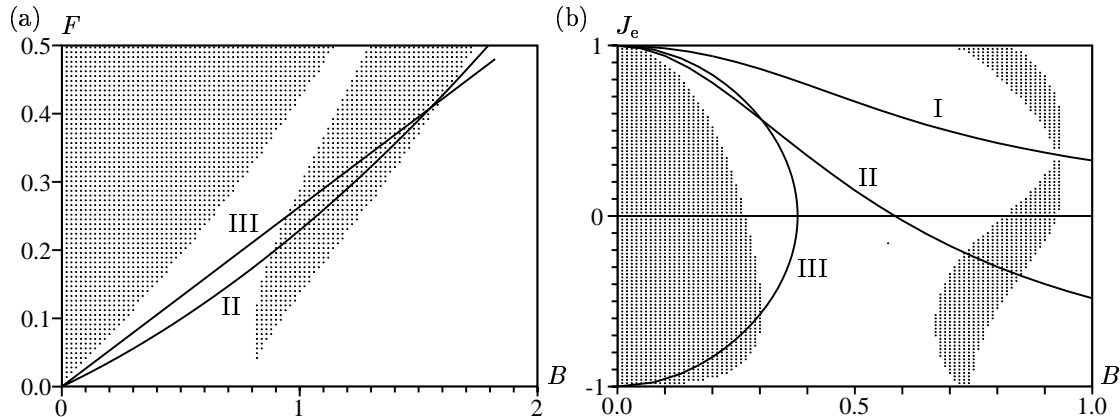
23

FIGURE 9. Stability diagrams of the equatorial orbit, obtained by computing numerically the multipliers of equation (105), starting with $w_e = \frac{\pi}{2}$ and different values of J_e, F and B. (a) shows the case $J_e = 0$ (b) the case $F = 0.1$. Shaded regions indicate unstable orbits. The curves are: I the location of the stable orbit (102), II the boundary (103) between regular and singular orbits (orbits with large B, large J_e or small F are regular), and III the stability boundary (93) of the doubly-averaged system.

orbits (102), for which both w_e and J_e are constant. In this case, we find $\det A > 0$, which means that the orbit is elliptic.

Fig. 9 shows numerically computed stability diagrams for general parameter values (one should note that equation (105) is much easier to treat numerically than the full equations of motion). As expected, orbits are unstable in a region compatible with condition (93) and stable for $B \gg F$. There appears to be a second zone of instability for intermediate values of $\frac{B}{F}$. However, this region corresponds to rather large values of B, for which the averaged Hamiltonian is not necessarily a good approximation. This confirms the picture that for small fields, the B-orbits are stable for small F and unstable for small B, with a linear transition line between both regimes.

4.4   The structure of phase space

The phase space of the averaged Hamiltonian is four-dimensional, and depends on the parameters Λ, F and B. The discussion in the previous sections suggests that the global structure of phase space will mainly depend on the ratio $\frac{B}{F}$; we expect that increasing both fields, while keeping their ratio constant, will mainly result in an increase of the size of chaotic components, without changing the location and stability of the main periodic orbits.

The equations of motion are given by (85), where the expressions of the linear and quadratic parts in B are deduced from (78) and (88) respectively. The manifold of constant energy is three-dimensional, and can be represented by a Poincaré section. The structure of the equations of motion shows that, at least when $\frac{B}{F}$ is not too large, a surface of section of the form $w_e = \text{constant}$ will be a good choice.

Fig. 10 shows Poincaré sections taken at $w_e = 0$ and $\frac{\pi}{2}$, in a case with $\frac{B}{F} = 1$ (sections with a smaller ratio of $\frac{B}{F}$ look similar). This section should be compared with Fig. 6a. The hyperbolic points located at $(w_K, K) = (\frac{\pi}{2}, 0)$ and $(\frac{3\pi}{2}, 0)$ correspond to the B-orbits. Their stable and unstable manifolds separate phase space into two regions, corresponding respectively to oscillations around the elliptic BF-orbits and around the S-orbits. In fact,
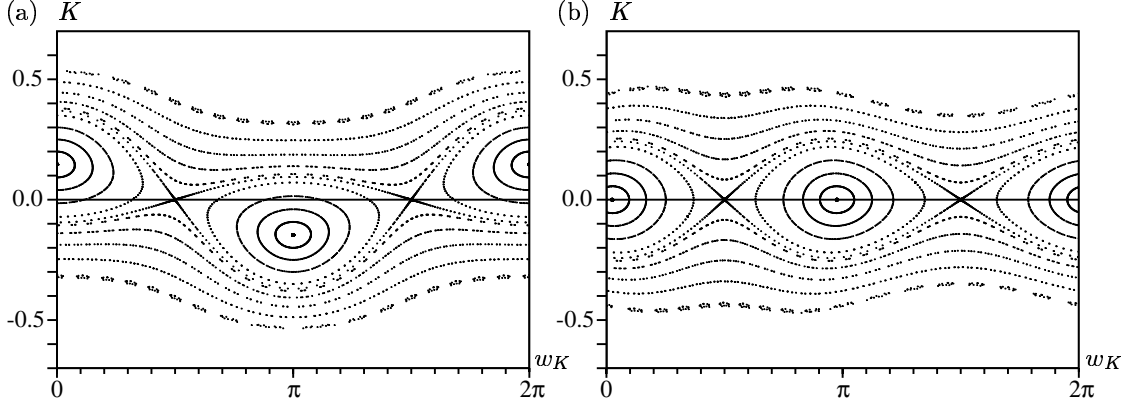
24

FIGURE 10. Poincaré sections of the singly-averaged Hamiltonian, (a) at $w_e = 0$ and (b) at $w_e = \frac{\pi}{2}$, for $B = F = 0.1$, $\Lambda = 1$ and $\langle H \rangle_\Lambda - H_0 = -0.15$ (which corresponds roughly to $J_e \simeq 0.5$). Hyperbolic points are the B-orbits, elliptic points the BF-orbits.
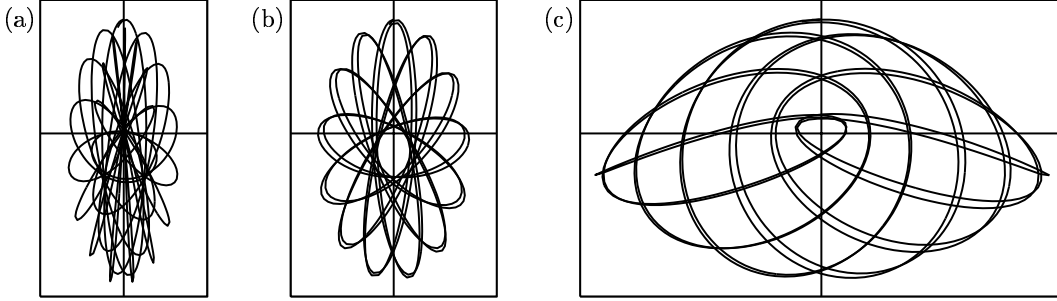

FIGURE 11. BF-orbits, obtained by integrating the equations of motion of the unaveraged Hamiltonian, (a) for $F = B = 0.05$ and (b,c) for $F = 0.05$ and $B = 0.1$. Initial conditions are given by (106) with $e = 0.2$. In (a) and (b), $\mathbf{F}$ is vertical and $\mathbf{B}$ points out of the plane, (c) shows a projection on the $(\mathbf{B}, \mathbf{F})$-plane.

we expect chaotic motions to show up near the separatrices, but they occupy a very small area for these values of the fields.

In contrast to the B-orbits, the BF-orbits move in the (w_K, K)-plane as w_e varies. This effect did not show up in the doubly-averaged approximation, and is mainly due to terms linear in B of the Hamiltonian. Fig. 10 shows that the BF-orbits are roughly located at $K \simeq \alpha \cos w_e$, $w_K \simeq \beta \sin w_e$ and $K \simeq -\alpha \cos w_e$, $w_K \simeq \pi - \beta \sin w_e$, where α and β are of order $\frac{B}{F}$ (they can be estimated by inserting Fourier series in the equations of motion).

In order to understand the geometry of BF-orbits, we observe that

1. if $w_e = 0$, K reaches its maximum and $w_K = 0$; we know by (64) that in this case the eccentricity is maximal and $\cos \omega = 0$; since $K \neq 0$, however, e is strictly smaller than 1, and thus the orbit no longer approaches the nucleus, as it does for $B = 0$; (80) shows that $\Omega = \frac{\pi}{2}$ or $\frac{3\pi}{2}$ (depending on the sign of J_e); this means that the plane of the Kepler ellipse contains $\mathbf{B} \wedge \mathbf{F}$, and since $\cos \omega = 0$, its major axis is in the plane $(\mathbf{B}, \mathbf{F})$.

2. if $w_e = \frac{\pi}{2}$, $K = 0$ and $w_K = \beta$; we also have $\cos \omega = 0$, but this time the eccentricity is minimal; (80) shows that $\sin \Omega = \mathcal{O}(\beta)$, meaning that the plane of the ellipse contains $\mathbf{F}$, but is slightly rotated with respect to the $(\mathbf{B}, \mathbf{F})$-plane, by an amount of order $\frac{B}{F}$.

In fact, when $\frac{B}{F}$ is small, we can deduce from (80) that Ω is close to 0 or π for most values of w_e. It approaches a step function of the form $\frac{\pi}{2}[1 - \text{sign}(\sin w_e)]$ as $\frac{B}{F}$ tends to zero,
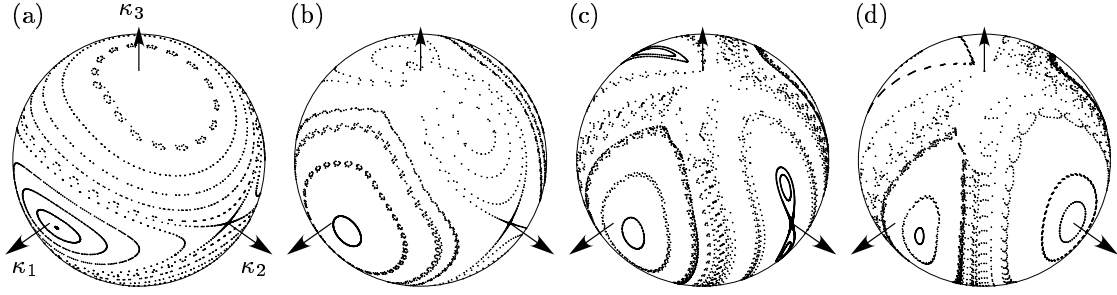
FIGURE 12. Poincaré sections at $w_e = \frac{\pi}{2}$ of the averaged system, represented on the sphere $\kappa_1^2 + \kappa_2^2 + \kappa_3^2 = (\Lambda - |J_e|)^2$ for increasing values of $\frac{B}{F}$, compare Fig. 6. In all cases, $\Lambda = 1$, $\langle H \rangle_\Lambda = -\frac{1}{2} - \frac{3}{2}F$, and $B = 0.1$. (a) $F = 0.1$, (b) $F = 0.05$, (c) $F = 0.038$ and (d) $F = 0.03$. Points are sparse near the poles, as we only plot points obtained with sufficient numerical accuracy.

which means that the orbit approaches the $(\mathbf{B}, \mathbf{F})$-plane in this limit. For increasing B, however, the orbit gains some thickness in the direction perpendicular to the plane, and rotates around $\mathbf{B}$ (Fig. 11). BF-orbits are thus truly non-planar when $B > 0$.

Initial conditions producing BF-orbits can be constructed in the following way. Pick an eccentricity $e \in [0, 1)$. Starting with $w_e = 0$, we have $K = 0$ and $\Omega = w_K = \beta$ can be read off the Poincaré section (though, the orbit being elliptic, starting with a slightly wrong w_K will not have dramatic consequences). Taking $M = 0$ as initial position on the ellipse, the initial conditions are then obtained from (11) to be

$$
\begin{aligned}
x &= 0 & p_x &= -\cos\Omega \frac{1}{\Lambda}\sqrt{\frac{1+e}{1-e}} \\
y &= 0 & p_y &= -\sin\Omega \frac{1}{\Lambda}\sqrt{\frac{1+e}{1-e}} \\
z &= \Lambda^2(1-e) & p_z &= 0.
\end{aligned}
\tag{106}
$$

We can also start with $w_e = 0$, $M = 0$, and read $K = \alpha$ off the Poincaré section, and take as initial conditions

$$
\begin{aligned}
x &= 0 & p_x &= -\frac{1}{\Lambda}\sqrt{\frac{1+e}{1-e}} \\
y &= \Lambda K\sqrt{\frac{1+e}{1-e}} & p_y &= 0 \\
z &= \Lambda\sqrt{\Lambda^2(1-e^2) - K^2}\sqrt{\frac{1+e}{1-e}} & p_z &= 0.
\end{aligned}
\tag{107}
$$

The boundaries of the section are given by the condition $|K| = \Lambda - |J_e|$, and depend on w_K and w_e because J_e is no longer constant. They correspond to the location of the S-orbit. The equations of motion become singular as $|K| \to \Lambda - |J_e|$, which makes unreliable the numerical computation of orbits approaching the S-orbit. This singularity can be tamed by a canonical transformation $(J_e, K; w_e, w_K) \mapsto (J_e, J; \phi, -w_K)$. In the case $K \to \Lambda - J_e$, $J_e \geqslant 0$, for instance, it is given by $J = \Lambda - J_e - K$ and $\phi = w_e - w_K$, the other cases being similar. We will not elaborate on this point here.

Fig. 12 and Fig. 13 show phase portraits for increasing values of $\frac{B}{F}$. They mainly differ by the behaviour of the B-orbit and its stable and unstable manifolds. While for small $\frac{B}{F}$, these manifolds connect the B-orbits (Fig. 10 and Fig. 12a), they connect each B-orbit to an S-orbit for larger $\frac{B}{F}$ (Fig. 12b and Fig. 13a,b). When this ratio increases further,
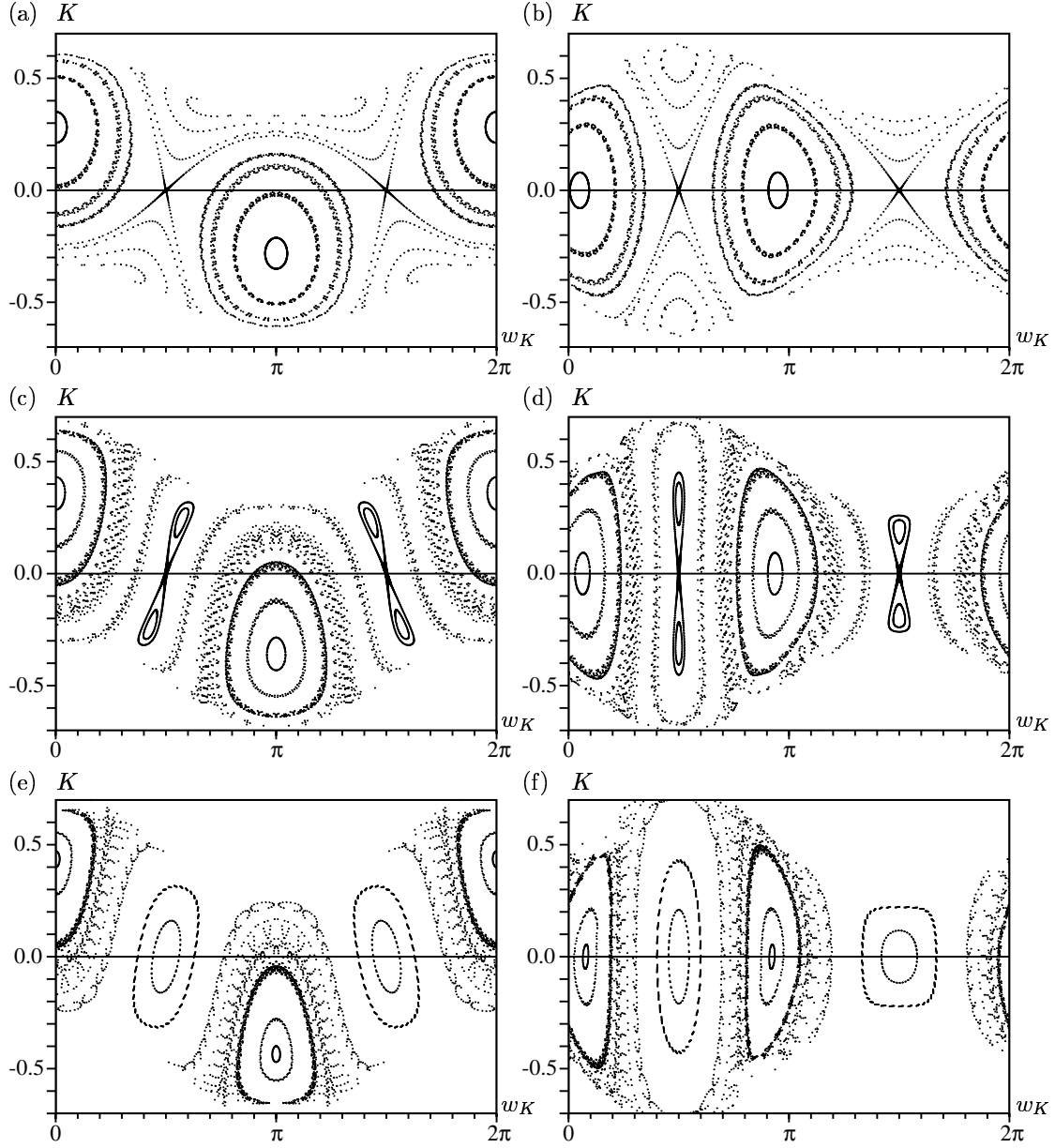
FIGURE 13. Poincaré sections of the averaged Hamiltonian for increasing values of $\frac{B}{F}$. (a,c,e) are taken at $w_e = 0$ and (b,d,f) at $w_e = \frac{\pi}{2}$. Values of Λ, H and B are the same as in Fig. 12, and (a,b) $F = 0.05$, (c,d) $F = 0.038$, (e,f) $F = 0.03$. The equilibrium points $K = 0$, $w_K = \frac{\pi}{2}$ and $\frac{3\pi}{2}$ are B-orbits, and the elliptic points near $w_K = 0, \pi$ are BF-orbits. The SB-orbits can be recognized on figures (b), (c) and (d).

27

each manifold folds back to the B-orbit it emerges from, enclosing an elliptic orbit that we called SB (Fig. 12c and Fig. 13c,d). Finally, the SB-orbits bifurcate with the B-orbit, which becomes elliptic, as we already know (Fig. 12d and Fig. 13e,f). This scenario is very close to the scenario obtained for the doubly-averaged system, compare Fig. 6.

The BF-orbit exists and remains elliptic for fairly large values of $\frac{B}{F}$. It is possible that it exists for all values of the field, and transforms into the Z-orbit or C-orbit of the Zeeman effect as $F \to 0$. Verifying this conjecture would, however, require an understanding of the transition between the Poincaré sections at $w_e = $ constant, valid for small and moderate $\frac{B}{F}$, and those at $\Omega' = $ constant, valid at large $\frac{B}{F}$. At least, it is true that the geometry of BF-orbits for $w_e = 0$ is compatible with that of the Z-orbits for $\Omega' = \frac{\pi}{2}$.

The structure of phase space is thus essentially organized around the B-orbits, BF-orbits and S-(or SB-)orbits, which are periodic orbits of the averaged Hamiltonian. The other orbits of the averaged system are either quasiperiodic with two frequencies, or belong to resonances or chaotic components, which are small, however, for the parameter values compatible with the averaging approximation. Intermediate values of $\frac{B}{F}$ are the most favorable for diffusion in phase space, as the heteroclinic connections between B- and S-orbits allow fast transitions between various regions of phase space.

The B-orbits are called S_+ and S_- by [FlWe96], who also describe a periodic orbit located in the plane perpendicular to $\mathbf{F}$, called $S_\perp$. We did not find such an orbit (which would correspond to $J_e = 0$ and $w_e = 0$ or π) in the parameter range we investigated. It might be that the BF-orbit behaves as the $S_\perp$-orbit for $F \ll B$.

Note that going from the averaged to the unaveraged dynamics will add a time scale. Hence, periodic orbits of the averaged system may correspond to quasiperiodic orbits of the unaveraged Hamiltonian with two frequencies, or to soft chaotic components. Some of the quasiperiodic orbits of the averaged system will support KAM-tori of the full system, which correspond to a quasiperiodic motion with three frequencies.

5   Conclusions and outlook

Action–angle variables and the technique of averaging help to understand the dynamics of the hydrogen atom in crossed electric and magnetic fields in two ways.

The first way is in terms of adiabatic invariants. The semi-major axis Λ^2 of the Kepler ellipse is a constant of motion of the averaged Hamiltonian, and thus an adiabatic invariant of the full Hamiltonian on the time scale B^{-2}, compare (82). The same role is played by the averaged perturbing function $\langle H \rangle_\Lambda - H_0$. In the case $B \ll F$, we have the additional invariants J_e and $\langle\langle H \rangle\rangle_{\Lambda, J_e}$ (see (88)), which evolve on the time scale B^{-1}. In the case $F \ll B$, $K' = \mathbf{L} \cdot \mathbf{B}/B$ and the averaged quadratic Zeeman term are adiabatic invariants on the time scale F^{-1}.

The second way is in terms of periodic orbits of the averaged system, which organize the structure of phase space. The B-orbits, contained in the plane perpendicular to $\mathbf{B}$, exist for all fields. They are unstable for $B \to 0$ and stable for $F \to 0$, with a roughly linear transition line in the (F, B)-plane. In the limit $B \to 0$, we also find the S-orbits of the Stark effect, and the stable BF-orbits contained in the plane of $\mathbf{B}$ and $\mathbf{F}$. As B increases, S-orbits appear to become unstable by expelling a pair of "SB-orbits", which are then absorbed by the B-orbits. BF-orbits are non-planar for $B > 0$. They exist and are stable in a large domain of field values. It is unclear whether they transform into one of the periodic orbits of the pure Zeeman effect as $F \to 0$.

Diffusion in phase space is most prominent in the regime where F and B are of comparable magnitude, when neighbourhoods of the S-orbits are connected by heteroclinic orbits. In the other regions of phase space, close to the stable orbits, orbits of the averaged system are trapped inside KAM-tori. In the real three-degrees-of-freedom system, however, diffusion becomes possible in these regions as well, although on a longer time scale. This aspect of dynamics still has to be better understood, as do the quantum and semiclassical mechanics of the problem which continue to be of interest [vMU97b, vMFU97b, N&97, RT97, CZRT99].

Acknowledgments

A   Averaging

A standard result on averaging [V96] is

Theorem A.1. *Consider the initial value problem*

$$\dot{x} = \varepsilon f(x,t) + \varepsilon^2 g(x,t,\varepsilon), \qquad x(0) = x_0, \tag{108}$$

where $f(x,t)$ is 2π-periodic in t, and $x, x_0 \in \mathbb{R}^n$. Define the averaged system

$$\dot{y} = \varepsilon \langle f \rangle(y), \qquad y(0) = x_0,$$
$$\langle f \rangle(y) = \frac{1}{2\pi} \int_0^{2\pi} f(y,t)\, \mathrm{d}t. \tag{109}$$

If f and g are sufficiently smooth and bounded, then

1. *$x(t) - y(t) = \mathcal{O}(\varepsilon)$ on the time scale $1/\varepsilon$;*
2. *If y_0 is a nondegenerate equilibrium of (109), then (108) possesses an isolated periodic orbit $\gamma(t) = y_0 + \mathcal{O}(\varepsilon)$, with the same stability as y_0 if y_0 is hyperbolic.*

Consider now a Hamiltonian of the form

$$H(I_1, \ldots, I_n; \varphi_1, \ldots, \varphi_n) = H_0(I_1) + \varepsilon H_1(I_1, \ldots, I_n; \varphi_1, \ldots, \varphi_n), \tag{110}$$

where the φ_i are angle variables. If we introduce the Poisson bracket

$$\{f; g\} = \sum_{i=1}^n \Big[\frac{\partial f}{\partial \varphi_i} \frac{\partial g}{\partial I_i} - \frac{\partial f}{\partial I_i} \frac{\partial g}{\partial \varphi_i} \Big], \tag{111}$$

the equations of motion can be written in the form

$$\begin{aligned}
\dot{\varphi}_1 &= H_0'(I_1) + \varepsilon\{\varphi_1; H_1\} \\
\dot{\varphi}_j &= \varepsilon\{\varphi_j; H_1\} & j &= 2, \ldots, n \\
\dot{I}_i &= \varepsilon\{I_i; H_1\} & i &= 1, \ldots, n.
\end{aligned} \tag{112}$$

If $\{\varphi_1; H_1\}$ is bounded, $H_0'(I_1) \neq 0$ and ε is small enough, we may reparametrize the orbits by φ_1 instead of t, giving

$$\frac{\mathrm{d}\varphi_j}{\mathrm{d}\varphi_1} = \varepsilon \frac{\{\varphi_j; H_1\}}{H_0'(I_1)} + \mathcal{O}(\varepsilon^2) \qquad j = 2, \ldots, n$$

$$\frac{\mathrm{d}I_i}{\mathrm{d}\varphi_1} = \varepsilon \frac{\{I_i; H_1\}}{H_0'(I_1)} + \mathcal{O}(\varepsilon^2) \qquad i = 1, \ldots, n.$$

(113)

According to the theorem, the dynamics of this system are well approximated by those of the system averaged over the fast variable φ_1,

$$\frac{\mathrm{d}\varphi_j}{\mathrm{d}\varphi_1} = \varepsilon \frac{\{\varphi_j; \langle H_1 \rangle\}}{H_0'(I_1)} \qquad j = 2, \ldots, n$$

$$\frac{\mathrm{d}I_i}{\mathrm{d}\varphi_1} = \varepsilon \frac{\{I_i; \langle H_1 \rangle\}}{H_0'(I_1)} \qquad i = 1, \ldots, n,$$

(114)

where we have introduced

$$\langle H_1 \rangle(I_1, \ldots, I_n; \varphi_2, \ldots, \varphi_n) = \frac{1}{2\pi} \int_0^{2\pi} H_1(I_1, \ldots, I_n; \varphi_1, \ldots, \varphi_n) \, \mathrm{d}\varphi_1. \qquad (115)$$

We now observe that the canonical equations associated with the averaged Hamiltonian $\langle H \rangle = H_0 + \varepsilon \langle H_1 \rangle$,

$$\dot{\varphi}_1 = H_0'(I_1) + \varepsilon \{\varphi_1; \langle H_1 \rangle\}$$
$$\dot{I}_1 = 0$$
$$\dot{\varphi}_j = \varepsilon \{\varphi_j; \langle H_1 \rangle\} \qquad\qquad\qquad j = 2, \ldots n \qquad (116)$$
$$\dot{I}_j = \varepsilon \{I_j; \langle H_1 \rangle\} \qquad\qquad\qquad j = 2, \ldots n$$

are close to $\mathcal{O}(\varepsilon^2)$ to those of the averaged system (114). Thus the dynamics of the averaged Hamiltonian are a good approximation, in the sense of the averaging theorem, of those of the initial Hamiltonian. In particular, the averaged Hamiltonian (115) is an adiabatic invariant of the initial system.

The averaging procedure can be extended to higher orders in ε by the method of Lie-Deprit series [D69, H70].

B   Poisson brackets

In this appendix, we discuss the computation of Poisson brackets involving various sets of variables used in this paper.

Since Hamiltonians are usually expressed in terms of auxiliary variables, such as the eccentricity e or inclination i, it is useful to start by computing some Poisson brackets involving these quantities. Some of them are shown in Table 3.

For instance, for the perturbation term $H_1 = \frac{1}{16} r^2 \left[1 + \cos^2 i + \sin^2 i \, \cos(2\omega + 2v) \right]$ of

30

	Λ	M	ω
e	0	$\dfrac{G^2}{\Lambda^3 e}$	$-\dfrac{G}{\Lambda^2 e}$
r	$-\dfrac{\Lambda^4 e}{r}\sin E$	$\dfrac{2r}{\Lambda} - \dfrac{G^2}{\Lambda e}\cos E$	$\dfrac{G}{e}\cos E$
$\sin^2 i$	0	0	$2\dfrac{K^2}{G^3}$
v	$-\dfrac{\Lambda^3 G}{r^2}$	$\dfrac{G\sin E}{re}$	$-\dfrac{\Lambda}{re}\sin E$
X	$\dfrac{\Lambda^4}{r}\sin E$	$-\dfrac{r^2}{e\Lambda^3} - \Lambda e\sin^2 E$	$\dfrac{G}{e}$
Y	$-\dfrac{\Lambda^3}{r}G\cos E$	$G\sin E$	$\Lambda\sin E$

TABLE 3. A few useful Poisson brackets involving Delaunay variables. We show Poisson brackets between columns and lines, for instance the upper right element is $\{\omega; e\}$. Brackets involving G, K and Ω are trivial to compute.

the Zeeman Hamiltonian, we find

$$\{\Lambda; H_1\} = -\frac{1}{8}\Lambda^4 e\big[1 + \cos^2 i + \sin^2 i\,\cos(2\omega + 2v)\big]\sin E + \frac{1}{8}\Lambda^3 G\sin^2 i\,\sin(2\omega + 2v)$$

$$\{G; H_1\} = \frac{1}{8}r^2\sin^2 i\,\sin(2\omega + 2v)$$

$$\{M; H_1\} = \frac{1}{8}r\Big(\frac{2r}{\Lambda} - \frac{G^2}{\Lambda e}\cos E\Big)\big[1 + \cos^2 i + \sin^2 i\,\cos(2\omega + 2v)\big]$$
$$\qquad - \frac{1}{8}\frac{rG}{e}\sin^2 i\,\sin(2\omega + 2v)\sin E$$

$$\{\omega; H_1\} = \frac{1}{8}\frac{rG}{e}\big[1 + \cos^2 i + \sin^2 i\,\cos(2\omega + 2v)\big]\cos E$$
$$\qquad + \frac{1}{8}\frac{r\Lambda}{e}\sin^2 i\,\sin(2\omega + 2v)\sin E + \frac{1}{8}\frac{r^2}{G}\big[-1 + \cos(2\omega + 2v)\big]. \tag{117}$$

There is an apparent singularity at $e = 0$. It can be removed, however, by introducing variables $J = \Lambda - G = \mathcal{O}(e^2)$ and $\phi = M + \omega$. The transformation $(\Lambda, G, K; M, \omega, \Omega) \mapsto (\Lambda, J, K; \phi, -\omega, \Omega)$ is canonical. One can check that $\dot\phi$ is finite in the limit $e \to 0$, and that the variable $\zeta = J\,e^{i\omega}$ satisfies $\dot\zeta = \mathcal{O}(e)$. This shows that the circular orbit is indeed a periodic orbit of the Zeeman Hamiltonian, as suggested by the averaged system.

Another way to deal with the singularity of Delaunay variables at $e = 0$ in the averaged case is to use coordinates (ξ_1, ξ_2, ξ_3) introduced by [CDMW87], see equation (24). Table 4 gives some useful Poisson brackets involving these variables.

C Angle variables to first order in F

For $F > 0$, the extremal values of ξ^2 are given by the condition

$$K^2 - 2\alpha_1(F)\xi^2 - 2H(F)\xi^4 + 2F\xi^6 = 0, \tag{118}$$

	ξ_1	ξ_2	ξ_3
ξ_1	0	$-2G\xi_3$	$2G\xi_2$
ξ_2	$2G\xi_3$	0	$-2G\xi_1$
ξ_3	$-2G\xi_2$	$2G\xi_1$	0
G	$-\xi_2$	ξ_1	0
e^2	$2\dfrac{1-e^2}{G}\xi_2$	$-2\dfrac{1-e^2}{G}\xi_1$	0
$\cos^2 i$	$2\dfrac{\cos^2 i}{G}\xi_2$	$-2\dfrac{\cos^2 i}{G}\xi_1$	0

TABLE 4. Some Poisson brackets involving the variables ξ_i defined in (24).

where the quantities

$$
\begin{aligned}
H(F) &= -\frac{1}{2\Lambda^2} - 3F\Lambda J_{\mathrm{e}} + \mathcal{O}(F^2)\\
\alpha_{1,2}(F) &= \frac{2J_{\xi,\eta} + K}{\Lambda} \pm F\Lambda^2\big[6J_\xi J_\eta + 3K(J_\xi + J_\eta) + K^2\big] + \mathcal{O}(F^2)
\end{aligned}
\tag{119}
$$

are obtained by solving equations (43) perturbatively. We find that ξ^2 varies between limits $\hat{a}_1(F) \pm \hat{b}_1(F)$ given by

$$
\begin{aligned}
\hat{a}_1(F) &= a_1 + \tfrac{1}{2}F\Lambda^4\big[J_{\mathrm{e}}^2 + 4\Lambda J_{\mathrm{e}} - 5\Lambda^2 + K^2\big] + \mathcal{O}(F^2)\\
\hat{b}_1(F) &= b_1\big[1 - \tfrac{1}{2}F\Lambda^3(5\Lambda + J_{\mathrm{e}})\big] + \mathcal{O}(F^2).
\end{aligned}
\tag{120}
$$

Likewise, the bounded orbits of η^2 vary between limits $\hat{a}_2(F) \pm \hat{b}_2(F)$ which are obtained by changing the signs of J_{e} and F in (120). We may parametrize the level curves of $\alpha_{1,2}$ by

$$
\begin{aligned}
\xi^2 &= \hat{a}_1(F) - \hat{b}_1(F)\cos\psi\\
\eta^2 &= \hat{a}_2(F) - \hat{b}_2(F)\cos\chi,
\end{aligned}
\tag{121}
$$

with the momenta given by (42). The derivatives of the action (54) can then be computed as before, with the result

$$
\begin{aligned}
w_\Lambda =&\frac{\psi + \chi}{2} - \frac{1}{2\Lambda^2}(b_1\sin\psi + b_2\sin\chi)\\
&+ \tfrac{1}{4}F\big[\Lambda(13\Lambda + 7J_{\mathrm{e}})b_1\sin\psi - b_1^2\sin 2\psi - \Lambda(13\Lambda - 7J_{\mathrm{e}})b_2\sin\chi + b_2^2\sin 2\chi\big]\\
&+ \mathcal{O}(F^2)\\
w_{\mathrm{e}} =&\frac{\chi - \psi}{2} + F\Lambda^2\big[b_1\sin\psi + b_2\sin\chi\big] + \mathcal{O}(F^2)\\
w_K =&\varphi - \rho_1(\psi) - \rho_2(\chi) + \tfrac{1}{2}FK\Lambda^4\Big[\frac{\sin\psi}{a_1 - b_1\cos\psi} - \frac{\sin\chi}{a_2 - b_2\cos\chi}\Big] + \mathcal{O}(F^2).
\end{aligned}
\tag{122}
$$

References

[B27]   M. Born, *The Mechanics of the Atom* (G. Bell, London, 1927).

[BM75]   A. Bohr, B.R. Mottelson, *Nuclear Structure, Vol. II* (Benjamin Reading, MA 1975).

[BS84]   P.A. Braun, E.A. Solov'ev, *The Stark Effect for a hydrogen atom in a magnetic field*, Sov. Phys. JETP **59**:38–46 (1984).

[C98]   J.-P. Connerade, *Highly Excited Atoms* (Cambridge U.P., Cambridge, UK, 1998).

[D69]   A. Deprit, *Canonical transformations depending on a small parameter*, Celestial Mech. **1**:12–30 (1969).

[CDMW87]   S.L. Coffey, A. Deprit, B. Miller, C.A. Williams, *The quadratic Zeeman Effect in Moderately Strong Magnetic Fields*, Ann. N.Y. Acad. Sci. **497**:22–36 (1987).

[CZRT99]   J.-P. Connerade, M.-S. Zhan, J. Rao, K.T. Taylor, *Strontium spectra in crossed electric and magnetic fields*, J. Phys. B **32**:2351–2360 (1999).

[DG89]   D. Delande, J.-C. Gay, *Quantum Chaos and the Hydrogen Atom in Strong Magnetic Fields* in G.F. Bassani, M. Inguscio, T.W. Hänsch Eds., *The Hydrogen Atom* (Springer-Verlag, Berlin, 1989).

[DK83]   R.J. Damburg, V.V. Kolosov, *Theoretical studies of hydrogen Rydberg atoms in electric fields* in R.F. Stebbings, F.B. Dunning Eds., *Rydberg states of atoms and molecules* (Cambridge Univ. Press, Cambridge, 1983).

[DKN83]   J.B. Delos, S.K. Knudson, D.W. Noid, *Highly excited states of a hydrogen atom in a strong magnetic field*, Phys. Rev. A **28**:7–21 (1983).

[DS92]   M.M. Dignam, J.E. Sipe, *Semiconductor superlattice exciton states in crossed electric and magnetic fields*, Phys. Rev. B **45**:6819–6838 (1992).

[DW91]   A. Deprit, C.A. Williams, *The Lissajous transformation. IV. Delaunay and Lissajous variables*, Celestial Mech. Dynam. Astronom. **51**:271–280 (1991).

[E16]   P.S. Epstein, Ann. Phys. **50**:489– (1916) Ann. Phys. **58**:553– (1919).

[F94]   D. Farrelly, *Motional Stark effect on Rydberg states in crossed electric and magnetic fields*, Phys. Lett. A **191**:265– (1994).

[F&92]   D. Farrelly, T. Uzer, P.E. Raines, J.P. Sketton, J.A. Milligan, *Electronic structure of Rydberg atoms in parallel electric and magnetic fields*, Phys. Rev. A **45**:4738–4751 (1992).

[FlWe96]   E. Flöthmann, K.H. Welge, *Crossed-field hydrogen atom and the three-body Sun-Earth-Moon problem*, Phys. Rev. A **54**:1884–1888 (1996).

[FrWi89]   H. Friedrich, D. Wintgen, *The hydrogen atom in a uniform magnetic field - an example of chaos*, Phys. Rep. **183**:37– (1989).

[G90]   M.C. Gutzwiller, *Chaos in Classical and Quantum Mechanics* (Springer-Verlag, New York, 1990).

[G98]   M.C. Gutzwiller, *Moon-Earth-Sun: The oldest three-body problem*, Rev. Mod. Phys. **70**:589–639 (1998).

[GT69]   W.R.S. Garton, F.S. Tomkins, Astrophys. J. **158**:839– (1969).

[H70]   J. Henrard, *On a perturbation theory using Lie transforms*, Celestial Mech. **3**:107–120 (1970).

[HRW89]   H. Hasegawa, M. Robnik, G. Wunner, *Classical and quantal chaos in the diamagnetic Kepler problem*, Progr. Theoret. Phys. Suppl. **98**:198–286 (1989).

[JFU99]   C. Jaffé, D.F. Farrelly, T. Uzer, *Transition state in atomic physics*, Phys. Rev. A **60**:3833–3850 (1999).

[JHY83]   B.R. Johnson, J.D. Hirschfelder, K.H. Yang, *Interaction of atoms, molecules, and ions with constant electric and magnetic fields*, Rev. Mod. Phys. **55**:109– (1983).

[KvL95]   P.M. Koch, K.A.H. van Leeuwen, *The importance of resonances in microwave "ionization" of excited hydrogen atoms*, Phys. Rep. **255**:289–406 (1995).

[L90]   J. Laskar, *The chaotic motion of the solar system: A numerical estimate of the size of the chaotic zones*, Icarus **88**:266–291 (1990).

[L96]   J. Laskar, *Large scale chaos and marginal stability in the solar system*, Celestial Mech. Dynam. Astronom. **64**:115–162 (1996).

[LR93]	J. Laskar, P. Robutel, *The chaotic obliquity of the planets*, Nature **361**:608–612 (1993).
[LL92]	A.J. Lichtenberg, M.A. Lieberman, *Regular and Chaotic Dynamics* (Springer-Verlag, New York, 1992).
[Ma89]	G. Mathys, Fundam. Cosm. Phys. **13**:143– (1989).
[Mi82]	F. Mignard, Icarus **49**:347– (1982).
[MW92]	J. Main, G. Wunner, *Ericson fluctuations in the chaotic ionization of the hydrogen atom in crossed magnetic and electric fields*, Phys. Rev. Lett. **69**:586–589 (1992).
[N&97]	C. Neumann *et al.*, *Symmetry breaking in crossed magnetic and electric fields*, Phys. Rev. Lett. **78**:4705–4708 (1997).
[R63]	P.J. Redmond, *Generalization of the Runge-Lenz Vector in the Presence of an Electric Field*, Phys. Rev. **133**:B1352–3 (1963).
[RFW91]	G. Raithel, M. Fauth, H. Walther, *Quasi-Landau resonances in the spectra of rubidium Rydberg atoms in crossed electric and magnetic fields*, Phys. Rev. A **44**:1898–1909 (1991).
[RFW93]	G. Raithel, M. Fauth, H. Walther, *Atoms in strong crossed electric and magnetic fields: Evidence for states with large electric-dipole moments*, Phys. Rev. A **47**:419–440 (1993).
[RT97]	J. Rao, K.T. Taylor, *Atoms in crossed fields: calculations for barium and hydrogen*, J. Phys. B **30**:3627–3645 (1997).
[Schw16]	K. Schwarzschild, *Sitzungsber. d. Berl. Akad. 1916*, p. 548.
[Schm93]	P. Schmelcher, *Delocalization of excitons in a magnetic field*, Phys. Rev. B **48**:14642–14645 (1993).
[S83]	E.A. Solov'ev, *Second-order perturbation theory for the hydrogen atom in crossed electric and magnetic fields*, Sov. Phys. JETP **58**:63–66 (1983).
[TLL79]	J.L. Tennyson, M.A. Lieberman, A.J. Lichtenberg, *Diffusion in Near-Integrable Hamiltonian Systems with Three Degrees of Freedom* in M. Month, J.C. Herrera Eds., *Nonlinear dynamics and the Beam–Beam Interaction* (Am. Inst. Phys. Conference Proceedings No. 57, New York, 1979). pp. 272-301.
[U&91]	T. Uzer *et al.*, *Celestial Mechanics on a Microscopic Scale*, Science **253**:42–48 (1991).
[UF95]	T. Uzer, D. Farrelly, *Threshold ionization dynamics of the hydrogen atom in crossed electric and magnetic fields*, Phys. Rev. A **52**:R2501–R2504 (1995).
[V96]	F. Verhulst, *Nonlinear Differential Equations and Dynamical Systems* (Springer-Verlag, Berlin, 1996).
[vMDU94]	J. von Milczewski, G.H.F. Diercksen, T. Uzer, *Intramanifold chaos in Rydberg atoms in external fields*, Phys. Rev. Lett. **73**:2428–2431 (1994).
[vMDU96]	J. von Milczewski, G.H.F. Diercksen, T. Uzer, *Computation of the Arnol'd Web for the hydrogen atom in crossed electric and magnetic fields*, Phys. Rev. Lett. **76**:2890–2893 (1996).
[vMFU97a]	J. von Milczewski, D. Farelly, T. Uzer, *$1/r$ Dynamics in External Fields: 2D or 3D?*, Phys. Rev. Lett. **78**:2349–2352 (1997).
[vMFU97b]	J. von Milczewski, D. Farelly, T. Uzer, *Role of the atomic Coulomb center in ionization and periodic orbit selection*, Phys. Rev. A **56**:657–670 (1997).
[vMU97a]	J. von Milczewski, T. Uzer, *Chaos and order in crossed fields*, Phys. Rev. E **55**:6540–6551 (1997).
[vMU97b]	J. von Milczewski, T. Uzer, *Canonical perturbation treatment of a Rydberg electron in combined electric and magnetic fields*, Phys. Rev. A **56**:220–231 (1997).
[W&89]	G. Wiebusch *et al.*, *Hydrogen atom in crossed magnetic and electric fields*, Phys. Rev. Lett. **62**:2821–2824 (1989).
[Y&93]	J.A. Yeazell *et al.*, *Observation of wave packet motion along quasi-Landau orbits*, Phys. Rev. Lett. **70**:2884–2887 (1993).